This is the peer-reviewed, final accepted version for American Mineralogist, published by the Mineralogical Society of America.
The published version is subject to change. Cite as Authors (Year) Title. American Mineralogist, in press.
DOI: https://doi.org/10.2138/am-2021-7647. http://www.minsocam.org/

Revision 2 (ms #7647R1)

Jingsuiite, TiB_2, a new mineral from the Cr-11 podiform chromitite orebody, Luobusa ophiolite, Tibet, China: Implications for recycling of boron

Fahui Xiong[1,2], Xiangzhen Xu[1], Enrico Mugnaioli[3], Mauro Gemmi[3], Richard Wirth[4], Edward S. Grew[5,*], and Paul T. Robinson[1]

[1]*Center for Advanced Research on the Mantle (CARMA), Key Laboratory of Deep-Earth Dynamics of Ministry of Land and Resources, Institute of Geology, Chinese Academy of Geological Sciences, Beijing 100037, China*

[2]*Southern Marine Science and Engineering Guangdong Laboratory (Guangzhou), Guangzhou, 511458, China*

[3]*Center for Nanotechnology Innovation@NEST, Istituto Italiano di Tecnologia, Pisa, 56127, Italy*

[4]*Helmholtz Centre Potsdam, GFZ German Research Centre for Geosciences, Section 3.5 Interface Geochemistry, Telegrafenberg, 14473 Potsdam, Germany*

[5]*School of Earth and Climate Sciences, University of Maine, Orono, Maine 04469 USA*

ABSTRACT

The new mineral jingsuiite (TiB_2, IMA-2018-117b), together with osbornite-khamrabaevite solid solution (TiN-TiC), deltalumite and a potential new mineral, hexagonal $Ti_{10}(Si,P,\square)_7$, constitute four inclusions up to 50 μm across in corundum recovered from the Cr-11 podiform chromitite orebody near Kangjinla, Luobusa ophiolite, Tibet, China. EELS, EDS and 3D electron diffraction were applied to study the phases. In one inclusion, jingsuiite forms a rounded grain 40 μm across. Associated osbornite-khamrabaevite solid solution forms an irregular mass up to 10 μm across having the composition $Ti(N_{0.5}C_{0.5})$ and the $Ti_{10}(Si,P,\square)_7$ phase forms an incomplete overgrowth up to 20 μm thick around the grain of jingsuiite. In a second inclusion, jingsuiite, osbornite-khamrabaevite solid solution, $Ti_{10}(Si,P,\square)_7$ and

Always consult and cite the final, published document. See http:/www.minsocam.org or GeoscienceWorld

This is the peer-reviewed, final accepted version for American Mineralogist, published by the Mineralogical Society of America.
The published version is subject to change. Cite as Authors (Year) Title. American Mineralogist, in press.
DOI: https://doi.org/10.2138/am-2021-7647. http://www.minsocam.org/

deltalumite form a lamellar intergrowth 100 μm long composed of tablets of the three phases up to 50 μm long x 4 μm in thickness. Jingsuiite has a primitive hexagonal cell with a = 3.04(6), b = 3.04(6), c = 3.22(6) Å, α = 90°, β = 90°, γ = 120°, V = 25.8 (9) Å^3, space group $P6/mmm$, Z = 1. Its structure was determined ab-initio and dynamically refined on the basis of 3-dimension electron diffraction data; it is equivalent to that of synthetic TiB_2. Results of EELS analyses of jingsuiite in foil #5357 (N = 20) gave B 61.87(1.22), C 1.53 (1.26), Ti 36.62 (1.45) atomic% from which an empirical formula of $Ti_{1.10}(B_{1.86}C_{0.05})_{\Sigma 1.91}$ was calculated on the basis of 3 atoms. The ideal formula is TiB_2. Our preferred scenario is that corundum with entrapped Ti-Si-P-Fe intermetallic melts was precipitated from basaltic magmas during exhumation following deep subduction. Enrichment of B in the melt pockets is attributed to the highly reducing conditions that led to the segregation of siderophile elements into intermetallic melts and to the siderophile behavior of B, thereby concentrating it in the intermetallic melts in preference to silicate melt. Experimental work on the Ti-Fe-Si system indicates that minerals enclosed in corundum grains such as Ti, $FeTiSi_2$, and $TiSi_2$ could have crystallized from alloy melts at the lowest T accessible on the liquidus, i.e., <1300 ºC. The presence of TiB_2 in four inclusions in the Cr-11 ore body suggests incorporation of crustal sediments in the ophiolite followed by deep subduction to the Transition Zone where qingsongite (cubic BN) is inferred to have crystallized and subsequently exhumed to shallower levels where hexagonal BN and jingsuiite presumably crystallized.

Keywords: boron, jingsuiite, intermetallic melts, crystal structure, transmitting electron microscopy, 3-dimensional electron diffraction

*E-mail: esgrew@maine.edu

Introduction

Boron is a quintessential crustal element. Of the 300 known minerals containing essential B, qingsongite, cubic BN, is the first B mineral believed to have originated in Earth's mantle (Dobrzhinetskaya et al. 2009, 2014). It occurs in trace amounts with osbornite (TiN) in a kyanite and coesite-bearing zone adjacent to a rim of α-Ti (native

Always consult and cite the final, published document. See http:/www.minsocam.org or GeoscienceWorld

This is the peer-reviewed, final accepted version for American Mineralogist, published by the Mineralogical Society of America.
The published version is subject to change. Cite as Authors (Year) Title. American Mineralogist, in press.
DOI: https://doi.org/10.2138/am-2021-7647. http://www.minsocam.org/

titanium, Fang et al. 2013) surrounding a core of Fe-Ti alloy in a fragment less than 1 mm across extracted from the Cr-31 chromitite orebody, Luobusa ophiolite, Tibet (Fig. 1)(Yang et al. 2007). Dobrzhinetskaya et al. (2014) interpreted the fragment to be a hybrid consisting of crustal material subducted to 400-500 km depth, where mantle components were incorporated. Other super-reduced species extracted from the Cr-31 chromitite include linzhiite, $FeSi_2$ (Li et al. 2012) and zangboite, $TiFeSi_2$ (Li et al. 2009).

Super-reduced intermetallic phases have also been reported in the Cr-11 podiform chromitite orebody (Fig. 2), which located at an elevation of 5 300 m at 29°11′ N, 92°18′ E in the Kangjinla district, 11 km east of the Cr-31 chromitite orebody (Fig. 1). However, the mode of occurrence is very different – the phases are enclosed in vitreous corundum grains (Fig. 3) that were found in mineral separates prepared from 1100 kg of chromitite. Xu et al. (2009, 2013, 2018) reported compounds that appear to correspond to known minerals, such as native titanium (Feng et al. 2013), Ti-Fe-Si (probably zangboite, $FeTiSi_2$, Li et al. 2009), Ti-N (osbornite) and Ti-C (khamrabaevite), as well as several Ti-Si, Ti-Si-P and Ti-B phases. Our studies using 3-dimension electron diffraction have confirmed the identity of TiN and TiC intermetallic compounds as osbornite-khamrabaevite, which constitute a continuous solid solution (e.g., Duwez and Odell 1950), and another five intermetallic compounds as distinct minerals with the compositions TiB_2, $TiSi_2$, TiP, $Ti_{10}(Si,P,\square)_7$ and $Ti_{11}(Si,P)_{10}$. The first three have been approved by the International Mineralogical Association Commission on New Minerals, Nomenclature and Classification (IMA CNMNC) as new minerals, respectively jingsuiite (Xiong et al. 2019a, this paper), badengzhuite (Xiong et al. 2019b, 2020c) and zhiqinite (Xiong et al. 2019c, 2020c), while proposals for the latter two are being prepared for submission to the Commission.

Jingsuiite was first reported in 2016 as an unnamed TiB_2 phase in a similar suite of highly reduced phases, which subsequent studies have shown to include osbornite,

Always consult and cite the final, published document. See http:/www.minsocam.org or GeoscienceWorld

This is the peer-reviewed, final accepted version for American Mineralogist, published by the Mineralogical Society of America.
The published version is subject to change. Cite as Authors (Year) Title. American Mineralogist, in press.
DOI: https://doi.org/10.2138/am-2021-7647. http://www.minsocam.org/

khamrabaevite, tistarite, hibonite and several Ti-Fe-Si-P compounds occurring as inclusions in corundum from Mount Carmel, Israel (e.g., Griffin et al. 2016a, 2020; Q. Xiong et al. 2017).

Because of potential industrial applications, the compounds TiN-TiC, $TiSi_2$, Ti_5Si_3, Ti_5P_3, TiP and TiB_2, have all been synthesized, but largely at atmospheric pressure (e.g., Novotny 1963; Snell 1967; Murray et al. 1986, Munro 2000, Okamoto et al. 2013). Oxygen fugacities for their stability are estimated to be as much as 10 log units less than the iron-wüstite buffer (e.g., Xiong et al. 2020c). Although there is no reason why these highly reduced phases could not have formed at higher pressures implied by the presence of diamond recovered from the Cr-11 orebody (Xu et al. 2009, 2015), e.g., $TiSi_2$ and TiB_2 have been synthesized at pressures of 5.5 GPa or more (Li et al. 2013; Zhong et al. 2020), the occurrence of these phases in the Luobusa ophiolite has become increasingly controversial. Ballhaus et al. (2017, 2018) argued that the mix of highly reduced and ultrahigh pressure minerals could be the result of lightning strikes rather than exhumation of material from deep in the mantle. Their argument is supported by the presence of similarly highly reduced phases in fulgurites, e.g., Essene and Fisher (1986, summarized in Hawthorne et al. 1988) described phases similar to those reported from the Luobusa ophiolite: stoichiometric TiP (could be badengzhuite) and quasi-stoichiometric $FeTi(Si,P)_2$ (could be P-bearing zangboite) on the basis of electron microprobe analysis.

However, Ballhaus et al. (in press) went further in reporting new experimental evidence interpreted to exclude the possibility of such highly reduced phases occurring in Earth's mantle. Furthermore, they noted that complex textures such as the symplectites involving Ti-Fe alloys and α-Ti in the qingsongite-bearing fragment (Yang et al. 2007; Fang et al. 2013; Dobrzhinetskaya et al. 2014) have unfavourable surface to volume ratios, and thus would be very unstable. In addition, on the basis of a detailed petrological and mineralogical study, Litasov et al. (2019a,b) contended that corundum grains enclosing the super-reduced phases in the Cr-11 chromitite orebody

Always consult and cite the final, published document. See http:/www.minsocam.org or GeoscienceWorld

This is the peer-reviewed, final accepted version for American Mineralogist, published by the Mineralogical Society of America.
The published version is subject to change. Cite as Authors (Year) Title. American Mineralogist, in press.
DOI: https://doi.org/10.2138/am-2021-7647. http://www.minsocam.org/

in the Luobusa ophiolite are brown fused alumina abrasive of anthropogenic origin, a contamination that was inadvertently introduced into separates prepared from the chromitite despite the great care taken, thereby providing evidence in support of the case being made by Ballhaus et al. (2017, 2018, in press).

After reviewing the arguments for and against a natural origin, Xiong et al. (2020c), concluded the preponderance of evidence favored a natural origin of the corundum grains and the highly reduced phases enclosed in these grains at Cr-11. As regards Cr-31, Dobrzhinetskaya et al. (2009, 2014) reported nitrogen isotopic evidence ($\delta^{15}N = -10.4 \pm 3‰$) for a deep mantle origin of a fragment containing both UHP minerals (coesite pseudomorphs after stishovite; TiO_2-II, the mineral srilankaite, which is included in coesite and kyanite) and highly reduced minerals (osbornite, α-titanium, Ti-Fe intermetallics, qingsongite).

Another leading question is whether B could have originated in recycled crustal material, which could be the source of B for qingsongite at mantle depths and for jingsuiite at shallower levels in the crust, as well as for the unnamed natural analogue of hexagonal BN reported in situ in chromitite from Cr-11 (Zhang et al. 2016). Another mineral from mantle depths reported to contain B at concentrations exceeding 1 ppm is type IIb blue diamond (1–8 ppm B, Gaillou et al. 2012). Smith et al. (2018) cited evidence that such B-bearing blue diamonds could have crystallized from fluids associated with deeply subducted crust.

Mineral name and type material

The TiB_2 mineral and its name jingsuiite have been approved by the IMA CNMNC (IMA2018-117b, Xiong et al. 2019a). The mineral was named in honor of Jingsui Yang (born June 6, 1950) of the Center for Advanced Research on the Mantle (CARMA), Key Laboratory for Continental Dynamics, Institute of Geology, Chinese Academy of Geological Sciences for his many contributions on the mineralogy of the chromitites associated with the Luobusa ophiolite. He was the Ph.D. advisor of the

Always consult and cite the final, published document. See http:/www.minsocam.org or GeoscienceWorld

This is the peer-reviewed, final accepted version for American Mineralogist, published by the Mineralogical Society of America.
The published version is subject to change. Cite as Authors (Year) Title. American Mineralogist, in press.
DOI: https://doi.org/10.2138/am-2021-7647. http://www.minsocam.org/

first author. Jingsui Yang has given his acceptance.

Type material is deposited in the collections of the Geological Museum of China, 15 Yangrouhutong, Xisi, West District, Beijing 100034, PR China, catalog number M13816.

Methods

Preparation of corundum separates from the Cr-11 chromitite and evidence for a natural origin of the corundum

Corundum and the unusual minerals included therein were extracted by processing ~1100 kg of chromitite at the Institute of Multipurpose Utilization of Mineral Resources, Chinese Academy of Geological Sciences, Zhengzhou, including massive, disseminated, and nodular ores from the Cr-11 orebody near Kangjinla, a process carried out with great care as described in detail by Xu et al. (2009, 2015). In brief, the samples were first passed through a jaw crusher and then ground in stages to three sizes, and the minerals were separated from each size fraction by a combination of gravity, magnetic and electrostatic techniques. The mineral concentrates were handpicked under a binocular microscope, and the selected minerals mounted in epoxy and then ground to about half their thickness. The grains were polished using man-made diamond grinding grease and cleaned in an ultrasonic bath. As far as we are aware, no industrial alumina was used at any stage of the extraction process.

Transmission electron microscopy and focused ion beam methodology

At the at GFZ Potsdam transmission electron microscopy (TEM) and focused ion beam (FIB) technology were used to determine the composition of the minerals included in corundum (for details of method in general, see Wirth 2004, 2009). TEM requires that samples be prepared as foils sufficiently thin to be transparent to electrons (generally, the foil thickness is less than 200 nm). Electron transparent foils were prepared with a FIB. Typical TEM foils have the dimensions 15×10×0.20 μm. A FIB single beam device (FEI FIB 200 TEM) was used for sample preparation. For this, a Ga-ion beam (30 keV acceleration voltage) is focused onto a selected location

Always consult and cite the final, published document. See http:/www.minsocam.org or GeoscienceWorld

This is the peer-reviewed, final accepted version for American Mineralogist, published by the Mineralogical Society of America.
The published version is subject to change. Cite as Authors (Year) Title. American Mineralogist, in press.
DOI: https://doi.org/10.2138/am-2021-7647. http://www.minsocam.org/

of the sample surface to sputter material from the sample.

Electron energy loss spectroscopy (EELS)

Measurement conditions for the EELS analysis of jingsuiite was carried out at the GFZ German Research Centre for Geosciences under the following conditions:

- 200 keV, diffraction mode
- camera length 650 mm
- dispersion 0.1 eV/channel
- collection angle, 4 mrad
- acceptance angle 10 mrad
- convergence half-angle: 2 mrad
- collection half-angle: 10 mrad
- acquisition time 30 x 1 second
- The 20 measurements covered the whole sample at constant thickness
- Model: Hartree Slater
- Background model: Power law
- 0.3 eV/channel
- Gatan software package.

Experimental: 3-dimensional electron diffraction and structure analysis

3-dimensional electron diffraction (3D ED) data (Gemmi et al. 2019) were acquired with a Zeiss Libra TEM operating at 120 kV and equipped with a LaB_6 source at the Istituto Italiano di Tecnologia (IIT), Center for Nanotechnology Innovation@NEST, Pisa. 3D ED was performed in STEM mode after defocusing the beam in order to have a parallel Köhler illumination on the sample. A beam size of about 150 nm in diameter was obtained by inserting a 5 μm C2 condenser aperture. An extremely low dose illumination was used in order to avoid any possible amorphization of the sample.

The best data collection used for structure solution and refinement was performed with an angular step of 1° and in total tilt range of 90° (from -50° to +40°). The useful

Always consult and cite the final, published document. See http:/www.minsocam.org or GeoscienceWorld

This is the peer-reviewed, final accepted version for American Mineralogist, published by the Mineralogical Society of America.
The published version is subject to change. Cite as Authors (Year) Title. American Mineralogist, in press.
DOI: https://doi.org/10.2138/am-2021-7647. http://www.minsocam.org/

tilt range was limited by the thickness of the FIB lamella. After each tilt, a diffraction pattern was acquired and crystal position tracked by defocused STEM imaging. During the experiment, the beam was precessed around the optical axis by an angle of 1° (Vincent and Midgley 1994), as first described by Mugnaioli *et al.* (2009). Precession was obtained using a Nanomegas Digistar P1000 device. Diffraction patterns were recorded by an ASI Timepix single-electron camera (Nederlof *et al.* 2013).

3D ED data were analyzed using the software PETS (Palatinus *et al.* 2019). Ab-initio structure determination was obtained by standard direct methods (SDM) as implemented in the software SIR2014 (Burla *et al.* 2015). Data were treated with a fully kinematical approximation, i.e. neglecting dynamical scattering and assuming that I_{hkl} was proportional to $|F_{hkl}|^2$. Least-squares structure refinement was performed with the software JANA2006 (Petříček et al. 2014) using the dynamical refinement procedure described by Palatinus *et al.* (2015). Only 29 out of 91 diffraction patterns, mostly belonging to the central part of the data set, were actually used for the refinement, because the quality of the high tilt patterns were severely spoiled by the absorption connected with the thickness of the FIB lamella. During the refinement process, the thickness of the lamella at 0° tilt was estimated in about 75 nm.

The visualization of the 3D ED data was obtained by the software ADT3D (Kolb *et al.* 2011) and structure sketches were drawn by the software VESTA (Momma and Izumi 2011).

Occurrence, appearance, morphology, physical and optical properties

Jingsuiite has been found in isolated grains or aggregates of intermetallics included in corundum as follows:

(1) The material used to characterize the mineral, including its crystal structure, is a rounded grain of jingsuiiite about 40 μm across associated with osbornite-khamrabaevite solid solution close to the midpoint in composition, $Ti(C_{0.5}N_{0.5})$, and a potential new mineral, $Ti_{10}(Si,P,\square)_7$ (foil #5357, Fig. 4).

(2) A second rounded grain of jingsuiite, but only 10 μm across, is associated with

Always consult and cite the final, published document. See http:/www.minsocam.org or GeoscienceWorld

This is the peer-reviewed, final accepted version for American Mineralogist, published by the Mineralogical Society of America.
The published version is subject to change. Cite as Authors (Year) Title. American Mineralogist, in press.
DOI: https://doi.org/10.2138/am-2021-7647. http://www.minsocam.org/

a Ti-N phase (foil#4106, Fig. 5) originally reported as sample KCr-13-1-4 by Xu et al. (2013); identification of the Ti-B phase in foil #4106 as jingsuiite was confirmed by 3D electron diffraction.

(3) Jingsuiite is found with osbornite-khamrabaevite solid solution and the $Ti_{10}(Si,P,\square)_7$ phase in a lamellar intergrowth 50 μm long and 4 μm in thickness in foil #6034 (Fig. 6, 7). Identification of jingsuiite is based on EDX spectra (Fig. 8), on the indexing of a Fourier transform of an HREM image consistent with the TiB_2 structure, which was obtained on one of the tablets, and on 3-dimensional electron diffraction. A phase isostructural with dmisteigbergite, $(KCa_3)(Al_7Si_9)O_{32}$, is found in one area suggestive of a pool of melt between jingsuiite, the $Ti_{10}(Si,P,\square)_7$ phase and corundum (Fig. 7). A grain 1 μm long of deltalumite is surrounded by the $Ti_{10}(Si,P,\square)_7$ phase and jingsuiite.

(4) The fourth occurrence of jingsuiite is a planar grain 58 μm x 10 μm of TiB_2 in sample KCr-13-1-1 (Xu et al. 2018), the chemical composition of which is consistent with its identification as jingsuiite.

The relative orientation of the phases in the lamellar intergrowth enclosed by corundum in foil #6034 was determined by 3D ED and can be expressed as follows: jingsuiite (001) // osbornite (111) // deltaluminite (111) // dmisteinbergite-like mineral (001) // $Ti_{10}(Si,P,\square)_7$ (100). Beside sharing the (001) vector, jingsuiite and the dmisteinibergite-like phase structures are reciprocally rotated of about 90° around [001], so that jingsuiite (100) // dmisteinibergite-like (110) and jingsuiite (110) // dmisteinibergite-like (100). There is no obvious relationship between jingsuite and surrounding corundum. Moreover, corundum areas all have the same orientation, which implies that these areas belong to a single crystal.

No crystal faces are evident in the grains studied by us. Higashi and Atoda (1970) reported synthesis of crystals having four forms: hexagonal platelets showing large {001} faces, plates with {100} faces, needles elongated in the [110] direction and hexagonal prisms with distinct {100} and {001} faces. Griffin et al. (2020) show

Always consult and cite the final, published document. See http:/www.minsocam.org or GeoscienceWorld

This is the peer-reviewed, final accepted version for American Mineralogist, published by the Mineralogical Society of America.
The published version is subject to change. Cite as Authors (Year) Title. American Mineralogist, in press.
DOI: https://doi.org/10.2138/am-2021-7647. http://www.minsocam.org/

jingsuiite grains with a hexagonal outline or a tabular habit, but provide no crystallographic information on the visible forms.

Because jingsuiite is found only as a few grains not exceeding 50 μm across, characterization of its physical and optical properties must rely for the most part on observations of the synthetic analogue. The mineral is presumably opaque and black in color. Commercially available synthetic TiB_2 powder is dark-brown (product CAS# 12045-63-5) as is a TiB_2 sputtering target. Otani and Ishizawa (1994) reported (100) cleavage in a synthetic crystal.

Chemical data

The EDX spectra for foils #5357 and #6034 show peaks for boron (B), titanium (Ti) and carbon (C), but the signal at C is subordinate (Fig. 8). The Cu and Ga peaks in the spectra originated from the Cu-grid and from Ga implantation during the TEM foil preparation with the focused ion beam (FIB). The presence of B and Ti was additionally verified with electron energy loss spectroscopy (EELS, Fig. 9).

Analysis of the planar grain in sample KCr-13-1-1 (fourth occurrence cited above) with the JEOL JXA-8100 electron microprobe analyzer at the Key Laboratory of Nuclear Resources and Environment, East China Institute of Technology, gave B 29.55, Ti 68.66, Mn 0.03, Fe 0.02, Zr 0.08 Sum 98.33 wt% (Xu et al., 2018), close to the ideal composition B 31.1, Ti 68.9 wt %. P, N, Cr, Si, V, C were sought but not detected.

The Ti $L_{3,2}$-edge onset at 456 eV in the EELS spectrum (Fig. 9) for jingsuiite in foil#5357 is consistent with the presence of Ti as Ti^{2+} (Stoyanov et al., 2007; Griffin et al. 2020). Results of EELS analyses of jingsuiite in this foil (N = 20, Table 1) gave an empirical formula of $Ti_{1.10}(B_{1.86}C_{0.05})_{\Sigma 1.91}$ calculated on the basis of 3 atoms. However, the presence of C and N in the spectrum (Fig. 9) suggests the beam hit

Always consult and cite the final, published document. See http:/www.minsocam.org or GeoscienceWorld

This is the peer-reviewed, final accepted version for American Mineralogist, published by the Mineralogical Society of America.
The published version is subject to change. Cite as Authors (Year) Title. American Mineralogist, in press.
DOI: https://doi.org/10.2138/am-2021-7647. http://www.minsocam.org/

osbornite-khamrabaevite solid solution, $Ti(C_{0.5}N_{0.5})$ located nearby (Fig. 4). The ideal formula is TiB_2 and the corresponding wt% are B 31.1, Ti 68.9. We attribute the wide range of values, high standard deviations and the presence of C and N in the spectrum to the grain being very small relative to the beam size, which resulted in the beam striking associated phases.

Crystallography

3D electron diffraction of the material in foil #5357 (Fig. 10) gave a primitive hexagonal cell with a = 3.04(6), b = 3.04(6), c = 3.22(6) Å, α = 90°, β = 90°, γ = 120°, V = 25.8 (9), Z = 1. No further extinctions were detected, making the space group *P*6/*mmm* (#191) very probable. The ab-initio structure solution based on 3D ED data (CCDC Deposition Number 2046670) confirms indeed jingsuiite as the natural analogue of synthetic TiB_2 (AlB_2 structure type, Ehrlich, 1947, 1949; Zacharison, 1949; Kiessling, 1950; Tian et al., 2018), consistent with the crystal structure of jingsuiite from Mount Carmel determined by X-ray diffraction (Griffin et al. 2020).

The jingsuiite structure comprises alternating layers of Ti and B atoms (Fig. 11). Both atoms occupy crystallographic special positions (1*a* and 2*d*, respectively) with no positional degrees of freedom. Titanium atoms are arranged in a hexagonal tiling and coordinated to twelve B atoms in a hexagonal-prismatic polyhedron. The only possible valences are +2 for Ti and -1 for B. The interatomic distance Ti-B in jingsuiite is 2.38(3) Å.

Discussion

Comparison with the Mount Carmel jingsuiite parageneses

The only other reported natural occurrence of TiB_2 is Mount Carmel, Israel (Griffin et al. 2016a, 2020). The paragenesis of jingsuiite at Mount Carmel is similar to that in the Cr-11 chromitite in that jingsuiite is found in aggregates of super-reduced

Always consult and cite the final, published document. See http:/www.minsocam.org or GeoscienceWorld

intermetallic compounds enclosed in corundum. In some places, the aggregates are associated with dmisteinbergite-like phases. However, the occurrences differ in the identity of many of the associated phases, number of occurrences and mineralogical and chemical diversity. Jingsuiite has been found only with osbornite-khramabaevite, deltalumite and the $Ti_{10}(Si,P,\square)_7$ phase in four samples from the Cr-11 chromitite. These phases all lie in the 6-component system Ti-B-C-N-P-Si with Cr, V, Mn, and Fe present in much subordinate amounts. In contrast, Griffin et al. (2020) reported a large number of relatively diverse assemblages involving not only osbornite-khramabaevite and a Mg-Al spinel resembling deltalumite, but also ZrP, TiS and several Fe-Ti silicides, including a $TiFe_2(Si,P)$ phase, as well as the oxides carmeltazite, hibonite and tistarite. The mineralogical diversity can be attributed in part to the chemical diversity of jingsuiite-bearing assemblages at Mount Carmel, in which Cr and V are major constituents in several phases.

Conditions of formation

Griffin et al. (2020) emphasized the role of melting in the origin of jingsuiite at Mount Carmel, where it is a widespread albeit minor constituent in melt pockets trapped in corundum aggregates, which are found as xenoliths in basalt in Cretaceous volcanoes. Textures are cited as evidence of immiscibility between metallic (Fe-Ti-C-Si) melts, Ti-(oxy)nitride melts and Ca-Al-Mg-Si-O "oxide" melts. The metallic melts commonly form spherules in oxide glass. Griffin et al. (2020) reported that jingsuiite crystallized predominantly from the metallic melts, and to a lesser extent from the oxide melts. The parageneses in the melt pockets of the xenoliths require oxygen fugacities 6 orders of magnitude more reducing than the iron-wüstite buffer; conditions they believed were generated by interaction between evolved silicate melts and mantle-derived CH_4+H_2 fluids near the crust-mantle boundary. Estimates of the pressure are constrained to be near 1 GPa by (1) the abundance of corundum since experiments in the model CaO-Al_2O_3-SiO_2 system indicate anorthite melts incongruently to give corundum only above 1 GPa (Hariya and Kennedy 1968,

This is the peer-reviewed, final accepted version for American Mineralogist, published by the Mineralogical Society of America.
The published version is subject to change. Cite as Authors (Year) Title. American Mineralogist, in press.
DOI: https://doi.org/10.2138/am-2021-7647. http://www.minsocam.org/

Goldsmith 1980, Ottonelli et al. 2013) and (2) the presence of grossite ($CaAl_4O_7$) in some highly reduced xenoliths, which implies that pressures should not have exceeded 1 GPa (Ottonelli et al. 2013). As regards temperature, Griffin et al. (2020) suggested it decreased from >1450°C to ca 1200°C by comparing the mineral parageneses in the melt pockets with experimental studies. Lastly, Griffin et al. (2020) concluded that under these highly reducing conditions B behaved mainly as a siderophile element with a strong preference for the metallic melts over the oxide melts.

Applying the scenario proposed for Mount Carmel to Luobusa ophiolite raises several questions. As pointed out by Griffin et al. (2020), the Luobusa and Mount Carmel parageneses have many features in common, notably evidence for intermetallic melts and silicate melts in pockets enclosed in corundum and association of jingsuiite with the minerals crystallized from the intermetallic melts. However, in contrast to Mount Carmel, the only evidence for silicate melts in the jingsuiite-bearing pockets is the dmisteinbergite-like mineral, which is found in nano-scale melt pools in foil #6034 (Fig. 7). A similar dmisteinbergite-like mineral forms a halo around an intermetallic spheroid in foil #5358 lacking jingsuiite; this spheroid is interpreted to be a droplet of Ti-Si-P melt (Xiong et al. 2020c). Compositionally, the dmisteinbergite-like mineral corresponds to an aluminous granodioritic melt (approximately 40% anorthite, 10% orthoclase, 5% $SrAl_2Si_2O_8$, 11% Al_2SiO_5 and 35% quartz, Xiong et al., 2020c). The dmisteinbergite-like mineral could have resulted from the quenching of this aluminous granodioritic melt consistent with the interpretation suggested for other occurrences of dmisteinbergite, the hexagonal analogue of anorthite, $CaAl_2Si_2O_8$, which crystallized metastably instead of feldspar during rapid cooling from a silicate melt (Krivovichev *et al.,* 2012; Zolotarev *et al.,* 2019). Less obvious is whether the granodioritic melt is from the larger magmatic body from which corundum precipitated as Griffin et al. (2020) interpreted the oxide melts at Mount Carmel to be. Instead, the granodioritic melt in foils #6034 and #5358 could have formed by exsolution of a much subordinate immiscible silicate melt from a dominantly

Always consult and cite the final, published document. See http:/www.minsocam.org or GeoscienceWorld

This is the peer-reviewed, final accepted version for American Mineralogist, published by the Mineralogical Society of America.
The published version is subject to change. Cite as Authors (Year) Title. American Mineralogist, in press.
DOI: https://doi.org/10.2138/am-2021-7647. http://www.minsocam.org/

intermetallic melt, and thus have a local origin. In this case, the granodioritic composition of these melts would give no indication of the composition of the presumably basaltic melt from which the corundum precipitated. We can only speculate that this melt was sufficiently close to anorthite in composition that the minimum pressure can be estimated from the experimental data to be 1 GPa when the melt cooled. Grossite has not yet been found in the Cr-11 chromitite, and thus there are no constraints on the upper limit of pressure.

We are not aware of any experimental work on ternary phases in the Ti-Si-P system, which best approximates the intermetallic phases in foil #5358, the most thoroughly characterized inclusion from the Cr-11 chromitite (Xiong et al. 2020c). However, we can draw an analogy with the Ti-Fe-Si system (Weitzer et al., 2008), in which ternary Ti-Fe-Si minerals were reported to crystallize at temperatures much lower than binary phases, i.e., 1034-1230 ºC. Consequently, it is likely ternary Ti-Si-P phases would crystallize at temperatures below the 1330 – 1600 °C indicated for $TiSi_2$ and TiP, respectively in the Ti-Si and Ti-P binaries (Xiong et al. 2020c).

To provide a broader context for interpreting the P-T conditions under which jingsuiite and other B minerals crystallized, we have adopted the P-T-t loop suggested by Griffin et al. (2016, Fig. 11) as the basis for discussion (Fig. 12). Several highly reduced minerals potentially could provide constraints on the P-T path during exhumation, the most likely time for jingsuiite to have crystallized. One is the unnamed natural analogue of the hexagonal modification of BN, which was reported in situ in chromitite at Cr-11 (Zhang et al. 2016). Hexagonal BN implies pressures did not exceed 4 GPa at ~1100 °C during exhumation (Fig. 12).

A second highly reduced indicator is native Ti, which has been found in two inclusions in corundum at Cr-11 (Xu et al. 2013, F. Xiong and R. Wirth, unpublished data), as well as at Cr-31 in the qingsongite-bearing fragment (Fang et al. 2013). The diffraction data reported by F. Xiong and R. Wirth are consistent with the α

Always consult and cite the final, published document. See http:/www.minsocam.org or GeoscienceWorld

This is the peer-reviewed, final accepted version for American Mineralogist, published by the Mineralogical Society of America.
The published version is subject to change. Cite as Authors (Year) Title. American Mineralogist, in press.
DOI: https://doi.org/10.2138/am-2021-7647. http://www.minsocam.org/

polymorph, which implies a temperature less than the α-β transition in Ti, i.e., less than 882 °C (Fig. 12; Murray 1990; Deweale et al. 2015). This temperature constraint could apply either to crystallization of the included assemblages or to later annealing that inverted β-Ti to α-Ti.

A similar ambiguity is encountered in applying Ti polymorphism to estimate P-T conditions from native Ti associated with texturally complex symplectic intergrowths of several Ti-Fe intermetallics. Fang et al. (2013) reported powder X-ray diffraction data consistent with the α polymorph. Ballhaus et al. (in press) suggested that such complex textures have unfavourable surface to volume ratios, and thus would be very unstable and not be expected in material subjected to mantle conditions. In our view, the complex intergrowths of α-Ti with several different Fe-Ti alloys suggests the possibility that the metal portion of the qingsongite-bearing fragment at the deepest levels consisted dominantly of β-Ti, which broke down during exhumation to give α-Ti. Unlike α-Ti, the β polymorph can incorporate significant Fe (Murray 1990), which could account for the appearance of Fe-Ti phases associated with α-Ti in the qingsongite-bearing fragment.

Source and recycling of boron

Three B minerals have been reported from the Luobusa ophiolite: qingsongite, cubic BN, in a loose fragment from Cr-31 (Dobrzhinetskaya et al. 2009, 2014), hexagonal BN enclosed in chromite from chromitite Cr-11 (Zhang et al. 2016) and jingsuiite. A fourth B mineral, B carbide, has been reported from the qingsongite-bearing fragment, but it has not been characterized (Dobrzhinetskaya et al. 2009, 2014).

The paragenesis of the three minerals couldn't be more different. Qingsonite is associated with coesite pseudomorphs after stishovite, kyanite and "TiO_2 II", which is the TiO_2 end member of srilankaite (Tschauner et al. 2020). The assemblage stishovite-kyanite-srilankaite constrains pressures to `12 GPa or 400 km depth, which is close to the upper boundary of the Transition Zone (Fig. 12 from Dobrzhinetskaya

Always consult and cite the final, published document. See http:/www.minsocam.org or GeoscienceWorld

This is the peer-reviewed, final accepted version for American Mineralogist, published by the Mineralogical Society of America.
The published version is subject to change. Cite as Authors (Year) Title. American Mineralogist, in press.
DOI: https://doi.org/10.2138/am-2021-7647. http://www.minsocam.org/

et al. 2014). The N and C in associated osbornite, Ti(N,C), have a mantle isotopic signature, $\delta^{15}N = -10.4 \pm 3‰$ and $\delta^{13}C = +5 \pm 7‰$ (Dobrzhinetskaya et al. 2009, 2014), and thus the N composing qingsongite was also sourced in the mantle. In our view, the scenario proposed by Dobrzhinetskaya et al. (2009, 2014) is valid, that is, the silicate-nitride portion of the fragment sourced crustal material for Al and B and mantle material for N and C, thereby showing that B-bearing crustal material had been subducted deeply into the mantle and subsequently exhumed, as indicated by the green arrows in Figure 12. Replacement of stishovite by coesite and the presence of α-Ti instead of β-Ti implies that the fragment was subjected to partial recrystallization during exhumation.

Zhang et al. (2016) reported hexagonal BN as an inclusion in chromite from Cr-11, from which it can be inferred B had been incorporated in the Cr-11 chromitite, most likely from mixing in of crustal material such as sediments prior to burial of the ophiolite and subsequent exhumation (Fig. 12). Thus, B could also have been available for incorporation in the intermetallic melts from which it was precipitated as TiB_2 (jingsuiite).

The enrichments indicated by the presence of jingsuiite as a major constituent in the melt pockets implies additional processes concentrating B in crustal rocks were at work. Griffin et al. (2020) concluded that the highly reducing conditions led to the segregation of siderophile elements into intermetallic melts and that B displays siderophile behavior, thereby concentrating it in the intermetallic melts in preference to silicate melt. Thus, two concurrent processes were concentrating B in intermetallic melts, which can better explain how B concentrations could reach the amount necessary for a B phase such as jingsuiite to crystallize.

Implications

The lithophile element B is generally taken to be quintessentially crustal, since it is

Always consult and cite the final, published document. See http:/www.minsocam.org or GeoscienceWorld

This is the peer-reviewed, final accepted version for American Mineralogist, published by the Mineralogical Society of America.
The published version is subject to change. Cite as Authors (Year) Title. American Mineralogist, in press.
DOI: https://doi.org/10.2138/am-2021-7647. http://www.minsocam.org/

greatly enriched in the upper continental crust relative to primitive mantle, 17 μg/g versus 0.019 μg/g, by processes such as weathering, adsorption onto clay minerals in marine sediments, partial melting of sedimentary rocks and differentiation of the resulting granitic melts (Grew 2017). However, under conditions six orders of magnitude more reducing than the iron-wüstite buffer, B becomes siderophile, much preferring intermetallic melts to silicate melts (Griffin et al. 2020). This switch in behavior has resulted in the crystallization of a B mineral in association with Ti intermetallics such as osbornite, khamrabaevite, $Ti_{10}(Si,P,\square)_7$, and Ti-Fe silicides during rapid exhumation from the upper mantle. In pursuing the implications of the siderophile behavior of B and of diamond growth in pools of metallic melt (Smith et al. 2016), Griffin et al. (2020) speculated that much of the B in the mantle could be held in intermetallic melts.

However, the possibility that siderophile behavior could also play a role in retaining B in crustal rocks being subducted has not yet been considered. The presence of qingsongite (cubic BN) in a fragment of crustal rock that had been buried at 400 km depth implies B can be recycled back to the mantle, yet how B is retained in the subducting slab is an open question. Dehydration and melting, the processes receiving the most attention for their impact on the subducted rocks, lead to extraction of B from the subducting slab (e.g., Grew 2017). Could the siderophile behavior of B under highly reducing conditions play a major role in retaining B in the subducted slab as it does in rapidly exhumed rocks at Mount Carmel and Cr-11? Although the minerals associated with qingsongite and N isotopes in osbornite indicate crystallization at 12 GPa at 400 km depth (Dobrzhinetskaya et al. 2014), there are several striking similarities between the qingsongite-bearing fragment and jingsuiite-bearing assemblages included in corundum. In both cases, the B mineral is associated with an osbornite-khmrabaevite solid solution and Ti-rich intermetallic phases resulting from crystallization under highly reducing conditions. The present-day assemblage in the qingsongite-bearing fragment does not preclude the possibility that at much shallower depths in the mantle during subduction (Fig. 12) the fragment was

Always consult and cite the final, published document. See http:/www.minsocam.org or GeoscienceWorld

This is the peer-reviewed, final accepted version for American Mineralogist, published by the Mineralogical Society of America.
The published version is subject to change. Cite as Authors (Year) Title. American Mineralogist, in press.
DOI: https://doi.org/10.2138/am-2021-7647. http://www.minsocam.org/

subjected to conditions sufficiently reducing and temperatures high enough for B behave as a siderophile element. In this setting, B could have been incorporated in a Ti-rich intermetallic alloy or melt. In other words, retention of B in deeply subducted crustal rocks could depend on exposure of these rocks to highly reducing conditions under which B behaves as a siderophile element.

Acknowledgments

This research was co-supported by the Second Tibetan Plateau Scientific Expedition and Research Program (No. 2019QZKK0801), the National Key Research and Development Project of China (No. 2016YFC0600310), Key Special Project for Introduced Talents Team of Southern Marine Science and Engineering Guangdong Laboratory (Guangzhou) (No. GML2019ZD0201), the National Natural Science Foundation of China (NNSFC; No. 41672046, 41641015, 41720104009, 41703036), the China Geological Survey (CGS; Project No. DD201190060), and the International Geological Correlation Project (IGCP-649).

We thank the two anonymous reviewers for constructive and detailed comments.

References

Akaogi, M., Oohata, M., Hojitani, H., and Kawaji, H. (2011) Thermodynamic properties of stishovite by low-temperature heat capacity measurements and the coesite stishovite transition boundary. American Mineralogist, 96, 1325–1330.

Ballhaus, C., Wirth, R., Fonseca, R.O.C., Blanchard, H., Pröll, W., Bragagni, A., Nagel, T., Schreiber, A., Dittrich, S., Thome, V., Hezel, D.C., Below, R., Cieszynski, H. (2017) Ultra-high pressure and ultra-reduced minerals in ophiolites may form by lightning strikes. Geochemical Perspectives Letters 5, 42-46.

Ballhaus, C., Fonseca, R.O.C., Bragagni, A. (2018) Reply to Comment on “Ultra-high pressure and ultra-reduced minerals in ophiolites may form by lightning strikes” by Griffin et al., 2018: No evidence for transition zone metamorphism in the Luobusa ophiolite. Geochemical Perspectives Letters, 7, 3-4.

Ballhaus, C., Helmy, H.M., Fonseca, R.O.C., Wirth, R., Schreiber, A., l, Jöns, N. (in press) Ultra-reduced minerals in ophiolites cannot come from Earth’s mantle. American Mineralogist.

Burla, MC, Caliandro, R., Carrozzini, B; Cascarano, GL; Cuocci, C; Giacovazzo, C;

Always consult and cite the final, published document. See http:/www.minsocam.org or GeoscienceWorld

This is the peer-reviewed, final accepted version for American Mineralogist, published by the Mineralogical Society of America.
The published version is subject to change. Cite as Authors (Year) Title. American Mineralogist, in press.
DOI: https://doi.org/10.2138/am-2021-7647. http://www.minsocam.org/

Mallamo, M; Mazzone, A; Polidori, G. (2015) Crystal structure determination and refinement via SIR2014. Journal of Applied Crystallography, 48, 306-309. DOI: 10.1107/S1600576715001132

Corrigan, F.R., and Bundy, F.P. (1975) Direct transitions among the allotropic forms of boron nitride at high pressures and temperatures. Journal of Chemical Physics, 63, 3812–3820.

Day, H.W. (2012) A revised diamond-graphite transition curve. American Mineralogist, 97, 53–62.

DeWeale, A., Stutzmann, V., Bouchet, J., Bottin, F., Occelli, F. and Mezouar, M. (2015) High pressure-temperature phase diagram and equation of state of titanium. Physical Review, B 91, 134108 DOI: 10.1103/PhysRevB.91.134108

Dobrzhinetskaya , L.F., Wirth, R., Yang, J., Hutcheon, I.D., Weber, P.K., and Green, H.W. II (2009) High-pressure highly reduced nitrides and oxides from chromitite of a Tibetan ophiolite. Proceedings of the National Academy of Sciences, 106, 19233–19238.

Dobrzhinetskaya, L.F., Wirth, R., Yang, J., Green, H.W., Hutcheon, I.D., Weber, P.K. and Grew, E.S. (2014) Qingsongite, natural cubic boron nitride: The first boron mineral from the Earth's mantle. American Mineralogist, 99, 764-772.

Duwez, P. and Odell, F. (1950) Phase relationships in the binary systems of nitrides and carbides of zirconium, columbium, titanium, and vanadium. Journal of the Electrochemical Society, 97, 299-304.

Ehrlich, P. (1947) Beiträge zur Chemie des Titans. Angewandte Chemie A, 59(5/6), 163 (abstract).

Ehrlich, P. (1949) Über die binären Systeme des Titans mit den Elementen Stickstoff, Kohlenstoff, Bor und Beryllium. Zeitschrift für anorganische Chemie, 259, 1-41.

Essene, E. J., and Fisher, D.C. (1986) Lightning strike fusion: Extreme reduction and metal-silicate liquid immiscibility. Science, 234, 189-193. https://doi.org/10.1126/science.234.4773.189.

Fang Q, Bai W, Yang J, Rong H, Shi N, Li G, Xiong M, Ma Z (2013) Titanium, Ti, a new mineral species from Luobusha, Tibet, China. Acta Geologica Sinica 87, 1275-1280

Filonenko, N.E., Lavrov, I.V. (1958) Petrography of the Artificial Abrasives. Mashgiz, Moscow (90 pp., in Russian).

Gaillou, E., Post, J.E., Rost, D., and Butler, J.E. (2012) Boron in natural type IIb blue diamonds: chemical and spectroscopic measurements. American Mineralogist, 97, 421 1-18.

Gemmi, M.; Mugnaioli, E.; Gorelik, T. E.; Kolb, U.; Palatinus, L; Boullay, P.; Hovmöller, S.; Abrahams, J. P. (2019) 3D electron diffraction : the nanocrystallography revolution. American Chemical Society Central Science, *5*, 1315-1329.

Goldsmith, J.R. (1980) The melting and breakdown reactions of anorthite at high pressures and temperatures. American Mineralogist, 65(3-4), 272-284

Grew, E.S. (2017) Boron: From cosmic scarcity to 300 minerals. Elements, 13(5),

Always consult and cite the final, published document. See http:/www.minsocam.org or GeoscienceWorld

This is the peer-reviewed, final accepted version for American Mineralogist, published by the Mineralogical Society of America.
The published version is subject to change. Cite as Authors (Year) Title. American Mineralogist, in press.
DOI: https://doi.org/10.2138/am-2021-7647. http://www.minsocam.org/

225-229.

Griffin, W.L., Gain, S.E.M., Adams, D.T., Huang, J.X., Saunders, M., Toledo, V., Pearson, N.J., and O'Reilly, S.Y. (2016a) First terrestrial occurrence of tistarite (Ti_2O_3): Ultra-low oxygen fugacity in the upper mantle beneath Mount Carmel, Israel. Geology, 44, 815-818.

Griffin, W.L., Afonso, J.C., Belousova, E.A., Gain, S.E., Gong, X.-H., González-Jiménez, J.M., Howell, D., Huang, J.X., McGowan, N., Pearson, N.J., Satsukawa, T., Shi, R., Williams, P., Xiong, Q., Yang, J.-S., Zhang, M. and O'Reilly, S.Y. (2016b) Mantle recycling: Transition Zone metamorphism of Tibetan ophiolitic peridotites and its tectonic implications. Journal of Petrology, 57, 655-684.

Griffin, W.L., Toledo, V. and O'Reilly, S.Y. (2019) Discussion of "Enigmatic super-reduced phases in corundum from natural rocks: Possible contamination from artificial abrasive materials or metallurgical slags" by Litasov et al. (Lithos, 340-341, p.181-190)

Griffin, W.L., Gain, S.E. M., Saunders, M., Bindi, L., Alard, O., Toledo, V., O'Reilly, S.Y. (2020) Parageneses of TiB_2 in corundum xenoliths from Mt Carmel, Israel: Siderophile behaviour of boron under reducing conditions. American Mineralogist, 105, 1609–1621.

Hariya, Y., Kennedy, G.C. (1968) Equilibrium study of anorthite under high pressure and high temperature. American Journal of Science, 266, 193–203

Hawthorne, F.C., Burke, E.A.J., Ercit, T.S., Grew, E.S., Grice, J.D., Jambor, J.L., Puziewicz, Roberts, A.C., and Vanko, D.A. (1988) New Mineral Names. American Mineralogist, 73, 189-199.

Higashi, I. and Atoda, T. (1970) Growth of titanium diboride single crystals in molten aluminum. Journal of Crystal Growth, 7, 251-253.

Kiessling, R. (1950) The borides of some transition elements. Acta Chemica Scandinavica, 4, 209-227.

Kolb U., Mugnaioli E., Gorelik T.E. (2011) Automated electron diffraction tomography - A new tool for nano crystal structure analysis. Crystal Research and Technology, vol. 46, (no. 6), pp. 542-554 https://doi.org/10.1002/crat.201100036|

Krivovichev, S.V.; Shcherbakova, E.P.; Nishanbaev, T.P. (2012) The crystal structure of svyatoslavite and evolution of complexity during crystallization of a $CaAl_2Si_2O_8$ melt: A structural automata description. Canadian Mineralogist, 50, 585–592

Leeman, W.P. and Sisson, V.B. (1996) Geochemistry of boron and its implications for crustal and mantle processes. Reviews of Mineralogy, 33, 645-708 (reprinted in 2002).

Li G, Fang Q, Shi N, Bai W, Yang J, Xiong M, Ma Z, Rong H (2009) Zangboite, $TiFeSi_2$, a new mineral species from Luobusha, Tibet, China, and its crystal structure, The Canadian Mineralogist 47, 1265-1274

Li G, Bai W, Shi N, Fang Q, Xiong M, Yand J, Ma Z, Rong H (2012) Linzhiite, $FeSi_2$, a redefined and revalidated new mineral species from Luobusha, Tibet, China.

Always consult and cite the final, published document. See http:/www.minsocam.org or GeoscienceWorld

This is the peer-reviewed, final accepted version for American Mineralogist, published by the Mineralogical Society of America.
The published version is subject to change. Cite as Authors (Year) Title. American Mineralogist, in press.
DOI: https://doi.org/10.2138/am-2021-7647. http://www.minsocam.org/

European Journal of Mineralogy, 24, 1047-1052

Li, C.Y., Yu, Z.H., Liu, H.Z., and Lü, T.Q. (2013) The crystallographic stability and anisotropic compressibility of C54- type $TiSi_2$ under high pressure. Journal of Physics and Chemistry of Solids, 74, 1291–1294, https://doi.org/10.1016/j.jpcs.2013.04.006

Litasov, K. D., Kagi, H. Bekker, T. B. (2019a) Enigmatic super-reduced phases in corundum from natural rocks: Possible contamination from artificial abrasive materials or metallurgical slags. Lithos 340–341 (2019) 181–190.

Litasov, K. D., Bekker, T. B. Kagi, H. (2019b) Discussion. Reply to the discussion of "Enigmatic super-reduced phases in corundum from natural rocks: Possible contamination from artificial abrasive materials or metallurgical slags" by Litasov et al. (Lithos, v.340–341, p.181–190) by W.L. Griffin, V. Toledo and S.Y. O'Reilly. Lithos 340–341 (2019) 181–190. Lithos, 348. DOI: 10.1016/j.lithos.2019.105170

Momma, K.; Izumi, F. (2011) VESTA 3 for three-dimensional visualization of crystal, volumetric and morphology data. Journal of Applied Crystallography, 44, 1272–1276.

Mugnaioli E., Gorelik T., Kolb U. (2009)"Ab initio" structure solution from electron diffraction data obtained by a combination of automated diffraction tomography and precession technique. Ultramicroscopy, 109, 758-765. doi: 10.1016/j.ultramic.2009.01.011

Munro, R.G. 2000 Material properties of titanium diboride. *Journal of Research of the* National Institute of Standards and Technology, 105, 709–720.

Murray, J.L. (1990) Fe-Ti (iron-titanium). In Massalski, T.B., Okamoto, H., Subramanian, P.R. and Kacprzak, L., eds., Binary Alloy Phase Diagrams, second edition. p. 1783-1786. William W. Scott, Jr., publisher. American Society of Materials International.

Murray, J.L., Liao, P.K. and Spear, K.E. (1986) The B-Ti (Boron-Titanium) System. Bulletin of Alloy Phase Diagrams, 7, 550-555.

Nederlof, I.; van Genderen, E.; Li, Y.; Abrahams, J. P. A (2013) Medipix quantum area detector allows rotation electron diffraction data collection from submicrometre three-dimensional protein crystals. Acta Crystallographica D, 69, 1223–1230.

Nowotny, H. (1963) Alloy chemistry of transition elements borides, carbides, nitrides, aluminides, and silicides. In Beck, P.A., editor, Electronic structure and Alloy Chemistry of the Transition Elements, p. 179-220. Wiley & Sons, New York, London.

Okamoto, H. (2013) N-Ti (Nitrogen-Titanium). Journal of Phase Equilibria and Diffusion, 34, 151–152.

Otani, S. and Ishizawa, Y. (1994) Preparation of TiB_2 single crystals by the floating zone method. Journal of Crystal Growth, 140, 451—453

Ottonello, G., Attene, M., Ameglio, D., Belmonte,D., Zuccolini, M.V., and Natali, M. (2013) Thermodynamic investigation of the $CaO–Al_2O_3–SiO_2$ system at high P and T through polymer chemistry and convex-hull techniques. Chemical

Always consult and cite the final, published document. See http:/www.minsocam.org or GeoscienceWorld

This is the peer-reviewed, final accepted version for American Mineralogist, published by the Mineralogical Society of America.
The published version is subject to change. Cite as Authors (Year) Title. American Mineralogist, in press.
DOI: https://doi.org/10.2138/am-2021-7647. http://www.minsocam.org/

Geology, 346, 81-92.

Palatinus, L.; Petříček, V.; Correa, C. A. (2015) Structure refinement using precession electron diffraction tomography and dynamical diffraction: theory and implementation. Acta Crystallographica A , 71, 235-244.

Palatinus, L.; Brázda, P., Jelínek, M., Hrdá, J., Steciuk G., Klementova M. (2019) Specifics of the data processing of precession electron diffraction tomography data and their implementation in the program *PETS2.0*. Acta Crystallographica B, 75, 512–522.

Petříček, V., Dušek, M. and Palatinus, L. (2014) Crystallographic computing system JANA2006: general features. Zeitschrift für Kristallographie, 229, 345–352.

Robinson, P.T., Trumbull, R.B., Schmitt, A., Yang, J.S., Li, J.W., Zhou, M.F., Erzinger, J., Dare, S. (2015) The origin and significance of crustal minerals in ophiolitic chromitites and peridotites. Gondwana Research 27, 486–506.

Schmidt, M.W., Poll, S., Comodi, P., and Zanazzi, P.F. (1997) High-pressure behaviour of kyanite: Decomposition of kyanite into stishovite and corundum. American Mineralogist, 82, 460–466.

Smith, E.M., Shirey, S.B., Nestola, F., Bullock, E.S., Wang, J., Richardson, S.H., and Wang, W. (2016) Large gem diamonds from metallic liquid in earth's deep interior. Science, 354, 1403-1405.

Smith, E.M., Shirey, S.B., Richardson, S.H., Nestola, F., Bullock, E.S., Wang, J., and Wang, W. (2018) Blue boron-bearing diamonds from Earth's lower mantle. Nature, 560, 84-87.

Snell, P.-O. (1967) The crystal structure of TiP. Acta Chemica Scandinavica, 27, 1773-1776.

Stoyanov, E., Langenhorst, F., and Steinle-Neumann, G. (2007) The effect of valence state and site geometry on Ti $L_{3,2}$ and O K electron energy-loss spectra of Ti_xO_y phases. American Mineralogist, 92, 577-586.

Tian, J., Zhao, Y., Wang, B., Hou, H. and Zhang, Y. (2018) The structural, mechanical and thermodynamic properties of Ti-B compounds under the influence of temperature and pressure: First principles study. *Materials Chemistry and Physics*, **209**, 200-207.

Tschauner, O., Ma, C., Lanzirotti, A. and Newville, M.G. (2020) Riesite, a new high pressure polymorph of TiO_2 from the Ries Impact Structure. Minerals 2020, 10, 78; doi:10.3390/min10010078

Vincent, R. and Midgley, P.A. (1994) Double conical beam-rocking system for measure(ment of integrated electron diffraction intensities. Ultramicroscopy, 53, 271-282

Weitzer, F., Schuster, J.C., Naka, M., Stein, F., Pulm, M. (2008) On the reaction scheme and liquidus surface in the ternary system Fe—Si—Ti. Intermetallics, 16, 273—282.

Wirth, R. (2004) Focused ion beam (FIB): a novel technology for advanced application of micro- and nanoanalysis in geosciences and applied mineralogy. European Journal of Mineralogy, 16, 863–877.

Wirth, R. (2009) Focused ion beam (FIB) combined with SEM and TEM: advanced

Always consult and cite the final, published document. See http:/www.minsocam.org or GeoscienceWorld

This is the peer-reviewed, final accepted version for American Mineralogist, published by the Mineralogical Society of America.
The published version is subject to change. Cite as Authors (Year) Title. American Mineralogist, in press.
DOI: https://doi.org/10.2138/am-2021-7647. http://www.minsocam.org/

analytical tools for studies of chemical composition, microstructure and crystal structure in geomaterials on a nanometre scale. Chemical Geology, 261, 217–229.

Withers, A.C., Essene, E.J., and Zhang, Y. (2003) Rutile/TiO_2II phase equilibria. Contributions to Mineralogy and Petrology, 145, 199–204.

Xiong, F.H., Yang, J.S., Robinson, P.T., Xu, X.Z., Liu, Z., Li, Y., Liu, F., Chen, S.Y., (2015) Origin of podiform chromitite, a new model based on the Luobusa ophiolite, Tibet. Gondwana Research, 27, 525–542.

Xiong, F., Xu, X., Mugnaioli, E., Gemmi, M., Wirth, R., Grew, E.S. and Robinson, P.T. (2019a) Jingsuiite, IMA 2018-117b. CNMNC Newsletter No. 52; Mineralogical Magazine, 83, https://doi.org/10.1180/mgm.2019.73

Xiong, F., Xu, X., Mugnaioli, E., Gemmi, M., Wirth, R., Grew, E. and Robinson, P.T. (2019b) Badengzhuite, IMA 2019-076. CNMNC Newsletter No. 52; Mineralogical Magazine, 83, https://doi.org/10.1180/mgm.2019.73

Xiong, F., Xu, X., Mugnaioli, E., Gemmi, M., Wirth, R., Grew, E. and Robinson, P.T. (2019c) Zhiqinite, IMA 2019-077. CNMNC Newsletter No. 52; Mineralogical Magazine, 83, https://doi.org/10.1180/mgm.2019.73

Xiong, F., Xu, X., Mugnaioli, E., Gemmi, M., Wirth, R., Grew, E.S. and Robinson, P.T. (2019d) Potential new titanium minerals in corundum from the Cr-11 chromitite orebody, Luobusa ophiolite, Tibet, China: Evidence for super-reduced mantle derived fluids? Geological Society of America Abstracts with Programs, 51, No. 5 doi: 10.1130/abs/2019AM-333493.

Xiong, F., Xu, X., Mugnaioli, E., Gemmi, M., Wirth, R., Grew, E.S. (2020a) $(K,Sr,\square)(Ca,\square)_3Al_6Si_{10}O_{32}$, a dmisteinbergite-like phase from the Luobusa ophiolite, China: Evidence for quenching at mantle depths? Goldschmidt Abstracts, 2928.

Xiong, F., Xu, X., Mugnaioli, E., Gemmi, M., Wirth, R., Grew, E.S. (2020b) $Ti_{10}(Si,P)_{6-7}$ and $Ti_{11}(Si,P)_{10}$, new phases from the Luobusa ophiolite, China: Implications for crystallization of Ti-Si-P melts. Goldschmidt Abstracts, 2929.

Xiong, F., Xu, X., Mugnaioli, E., Gemmi, M., Wirth, R., Grew, E.S., Robinson, P.T. and Yang, J. (2020c) Two new minerals, badengzhuite, TiP, and zhiqinite, $TiSi_2$, from the Cr-11 chromitite orebody, Luobusa ophiolite, Tibet, China: Evidence for super-reduced mantle-derived fluids? European Journal of Mineralogy, 32, 557-574.

Xiong, Q., Griffin, W.L., Huang, J.-X., Gain, S.E.M., Toledo, V., Pearson, N.J. and O'Reilly, S.Y. (2017) Super-reduced mineral assemblages in "ophiolitic" chromitites and peridotites: the view from Mount Carmel. European Journal of Mineralogy, 29, 557–570

Xu, X., Yang, J., Chen, S., Fang, Q. and Bai, W. (2009) Unusual Mantle Mineral Group from Chromitite Orebody Cr-11 in Luobusa Ophiolite of Yarlung-Zangbo Suture Zone, Tibet. Journal of Earth Science, 20, 284–302.

Xu, X.Z., Yang, J.S., Guo, G.L., Xiong, F.H. (2013) Mineral inclusions in corundum from chromitites in the Kangjinla chromite deposit, Tibet. Acta Petrologica Sinica 29 (6), 1867–1877 (in Chinese with English abstract).

Always consult and cite the final, published document. See http:/www.minsocam.org or GeoscienceWorld

This is the peer-reviewed, final accepted version for American Mineralogist, published by the Mineralogical Society of America.
The published version is subject to change. Cite as Authors (Year) Title. American Mineralogist, in press.
DOI: https://doi.org/10.2138/am-2021-7647. http://www.minsocam.org/

766 Xu, X.Z., Yang, J.S., Robinson, P.T., Xiong, F.H., Ba, D.Z., Guo, G.L. (2015) Origin
767 of ultrahigh pressure and highly reduced minerals in podiform chromitites and
768 associated mantle peridotites of the Luobusa ophiolite, Tibet. Gondwana
769 Research 27, 686–700
770 Xu, X.Z., Yang, J.S., Xiong, F.H., Guo, G.L. (2018) Characteristics of titanium-
771 bearing inclusions found in corundum of Luobusa podiform chromitite, Tibet.
772 Earth Science, 43(4), 1025-1037 (in Chinese with English abstract).
773 Yang, J.-S., Dobrzhinetskaya, L., Bai, W.J., Fang, Q.S., Robinson, P.T., Zhang, J. and
774 Green, H.W,. II (2007) Diamond- and coesite-bearing chromitites from the
775 Luobusa ophiolite, Tibet. Geology, 35; 875–878
776 Zachariasen, W.H. (1949) Crystal Chemical Studies of the 5f-Series of Elements.
777 VIII. Crystal Structure Studies of Uranium Silicides and of CeSi~, NpSi~ and
778 $PuSi_2$. Acta Crystallographica, 2, 94-99.
779 Zhang, R.Y., Yang, J.S., Ernst, W. G., Jahn, B.-M., Lizuka, Y., Guo, G.L., 2016.
780 Discovery of in situ super-reducing, ultrahigh-pressure phases in the Luobusa
781 ophiolitic chromitites, Tibet: New insights into the deep upper mantle and
782 mantle transition zone. American Mineralogist, 101, 1285-1294.
783 Zhong, S., Chen, C., Li, Z., Liu, Y, Liu, B., Wu, Y. (2020) In situ synthesis of
784 polycrystalline cubic boron nitride reinforced by different morphologic TiB_2.
785 Journal of Materials Engineering and Performance, 29, 3784-3791 DOI:
786 10.1007/s11665-020-04896-6
787 Zolotarev, A.A., Krivovichev, S.V., Panikorovskii, T.L., Gurzhiy, V.V., Bocharov, V.N.
788 and Rassomakhin, M.A. (2019) Dmisteinbergite, $CaAl_2Si_2O_8$, a Metastable
789 Polymorph of Anorthite: Crystal-Structure and Raman Spectroscopic Study of
790 the Holotype Specimen. Minerals, 9, 570; doi:10.3390/min9100570
791

Always consult and cite the final, published document. See http:/www.minsocam.org or GeoscienceWorld

This is the peer-reviewed, final accepted version for American Mineralogist, published by the Mineralogical Society of America.
The published version is subject to change. Cite as Authors (Year) Title. American Mineralogist, in press.
DOI: https://doi.org/10.2138/am-2021-7647. http://www.minsocam.org/

792 Table 1. Electron-energy-loss spectroscopic analyses (in atomic %) for jingsuiite in
793 foil #5357 (n = 20)

Constituent	Mean	Range	Stand. Dev.
B	61.87	58.65-63.08	1.22
C	1.53	0.00-6.17	1.26
Ti	36.62	34.97-41.00	1.45
Total	100.02		

794
795

Always consult and cite the final, published document. See http:/www.minsocam.org or GeoscienceWorld

This is the peer-reviewed, final accepted version for American Mineralogist, published by the Mineralogical Society of America.
The published version is subject to change. Cite as Authors (Year) Title. American Mineralogist, in press.
DOI: https://doi.org/10.2138/am-2021-7647. http://www.minsocam.org/

796

797 **Figure captions**

798 Figure 1. Map of the Luobusa ophiolite, Tibet showing the Cr-31 and Cr-11 chromitite
799 orebodies.

800

801 Figure 2. Exposure showing the Cr-11 chromitite orebody from which jingsuiite was
802 recovered. The chromitite is enveloped by dunite. The adit entrance is approximately
803 3 m high.

804

805 Figure 3. Photograph of corundum grains with inclusions recovered from the Cr-11
806 chromitite orebody, Luobusa ophiolite.

807

808

809 Figure 4 Images of jingsuiite. (a). Backscattered electron (BSE) image of corundum
810 fragments with inclusions of jingsuiite and other Ti compounds. The dark-grey
811 material is epoxy resin disk (the grains were handpicked and mounted in an epoxy
812 resin disk, and then polished). (b) BSE image of inclusion from which foil #5357 was
813 taken. The inclusion is composed of osbornite-khamrabaevite solid solution,
814 $Ti(C_{0.5}N_{0.5})$, a potentially new mineral, $Ti_{10}(Si,P,\square)_7$, and jingsuiite, TiB_2. (c) High-
815 angle annular dark-field (HAADF) image of foil #5357, showing areas of osbornite-
816 khamrabaevite solid solution, $Ti(C_{0.5}N_{0.5})$, a potentially new mineral, $Ti_{10}(Si,P,\square)_7$,
817 and jinguiite, TiB_2. The section shown in the HAADF image is perpendicular to the
818 surface shown in the BSE images. BSE images taken at the Center for Advanced
819 Research on the Mantle and images and the HAADF image obtained at the GFZ
820 German Research Centre for Geosciences.

821

822 Figure 5. Secondary electron images showing a corundum fragment (Al_2O_3) with
823 inclusions of jingsuiite and other Ti compounds. (a) The dark-grey material
824 surrounding corundum is epoxy (b) Enlargement of inclusion from which foil #4106
825 was taken, showing an unidentified Ti-N phase and jingsuiite, TiB_2, the identification

Always consult and cite the final, published document. See http:/www.minsocam.org or GeoscienceWorld

This is the peer-reviewed, final accepted version for American Mineralogist, published by the Mineralogical Society of America.
The published version is subject to change. Cite as Authors (Year) Title. American Mineralogist, in press.
DOI: https://doi.org/10.2138/am-2021-7647. http://www.minsocam.org/

826 of which was confirmed by 3D electron diffraction. Images taken at the Chinese
827 Academy of Geological Sciences.
828
829 Figure 6 (a) BSE image of jingsuiite, TiB_2, and associated osbornite-khamrabaevite,
830 Ti(N,C) and $Ti_{10}(Si,P,\square)_7$ in foil #6034. Yellow line – source of HAADF image in (b).
831 (b) High-angle annular dark-field image that is oriented perpendicular to the BSE
832 image. Areas labeled as TiB_2 have cell parameters consistent with jingsuiite. Yellow
833 rectangle is outline for Figure 7a. The section shown in the HAADF image is
834 perpendicular to the surface shown in the BSE image. BSE image taken at the Center
835 for Advanced Research on the Mantle. HAADF image taken at the GFZ German
836 Research Centre for Geosciences.
837
838 Figure 7. (a) Bright field image showing location of jingsuiite and the
839 dmisteinbergite-like mineral (b) High-angle annular dark-field image of a part of (a)
840 enlarged. The area found to be amorphous was most likely the dmisteinbergite-like
841 mineral whose crystal structure was destroyed by previous HRTEM analyses. Images
842 taken at the GFZ German Research Centre for Geosciences
843
844 Figure 8. Energy-dispersive X-ray spectra of jingsuiite in foils #5357 and #6034.
845 Spectra obtained at the GFZ German Research Centre for Geosciences.
846
847 Figure 9. Deconvolved electron energy-loss (EEL)-spectra of jingsuiite: (a) B *K*-edge
848 with the edge onset at 188 eV, C *K*-edge with edge onset at 284 eV and Ti-$L_{3,2}$ edge
849 onset at 456 eV and (b) C *K*-edge with edge onset at 284 eV, N *K*-edge with the edge
850 onset at 401 eV, and Ti $L_{3,2}$-edge onset at 456 eV.
851
852 Figure 10. 3D reconstruction of electron diffraction data taken from jingsuiite in foil
853 #5357. Images of the 3D reciprocal space along the most relevant crystallographic
854 directions in reciprocal space: 100*, 010*, 001* and 110*. These patterns are

Always consult and cite the final, published document. See http:/www.minsocam.org or GeoscienceWorld

projections of a 3D diffraction volume and are not conventional 2D SAED patterns. No systematic extinctions are visible. Unit cell is sketched in yellow. Vector ***a**** is in red, ***b**** is in green, ***c**** is in blue. Patterns were obtained at the Istituto Italiano di Tecnologia.

Figure 11. Crystal structure of jingsuiite. Blue – Ti; green – B. (a) [001] projection. (b) [100] projection. H = B atoms in an array approximating a hexagonal net; A = Ti atoms closely packed in a hexagonal tiling (cf. Kiessling 1950). Unit cell is outlined by black lines. Drafted with VESTA (Momma and Izumi 2011).

Figure 12. Pressure-temperature diagram summarizing evolution of the Luobusa ophiolite as it relates to the super-reduced minerals and B (modified from Griffin et al. 2016b, Fig. 11, Xiong et al. 2020c, Fig. 11) with *P-T* estimate for qingsongite, cubic BN, from Dobrzhenitskaya et al. (2014) shown as cube labeled cBN. Graphite ⇔ diamond (Gr-Dia) from Day (2012); hexagonal BN ⇔ qingsongite (hBN-cBN) from Corrigan and Bundy (1975, Fig. 3, "graphitization" line); coesite ⇔ stishovite (Coe-Sti) from Akaogi et al. (2011); rutile ⇔ srilankaite (Rt-Sri) from Withers et al. (2003); kyanite ⇔ stishovite + corundum (Ky-Sti + Crn) from Schmidt et al. 1997); triple point for titanium polymorphs (olive-green), α-Ti, β-Ti and ω-Ti modified from Deweale et al. (2015, Fig. 2). Boron for the unnamed natural analogue of hexagonal BN and jingsuite (hexagons labeled hBN and TiB_2, respectively) is interpreted to have been recycled through the mantle (green arrows, e.g., Zhang et al. 2016).

N

0 1 2 km

E92°12′

Yarlung Zangbo River

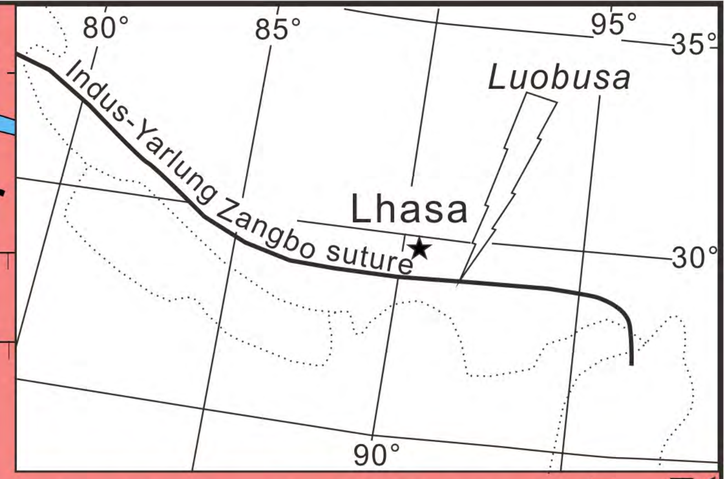

Cr

Cr-31

Cr

Cr

B

Luobusa

Cr

Shashen

Cr

Cr-11

Cr

A

B

Kangjinla

N29°10′

E92°18′

A

Granite

Tertiary Luobusa Formation

Upper Triassic Flysch

Upper Cretaceous Zedang Formation

Cumulate rock

Dunite

Harzburgite

Cr

Podiform chromitite

Unconformity

Fault

Thrust contact

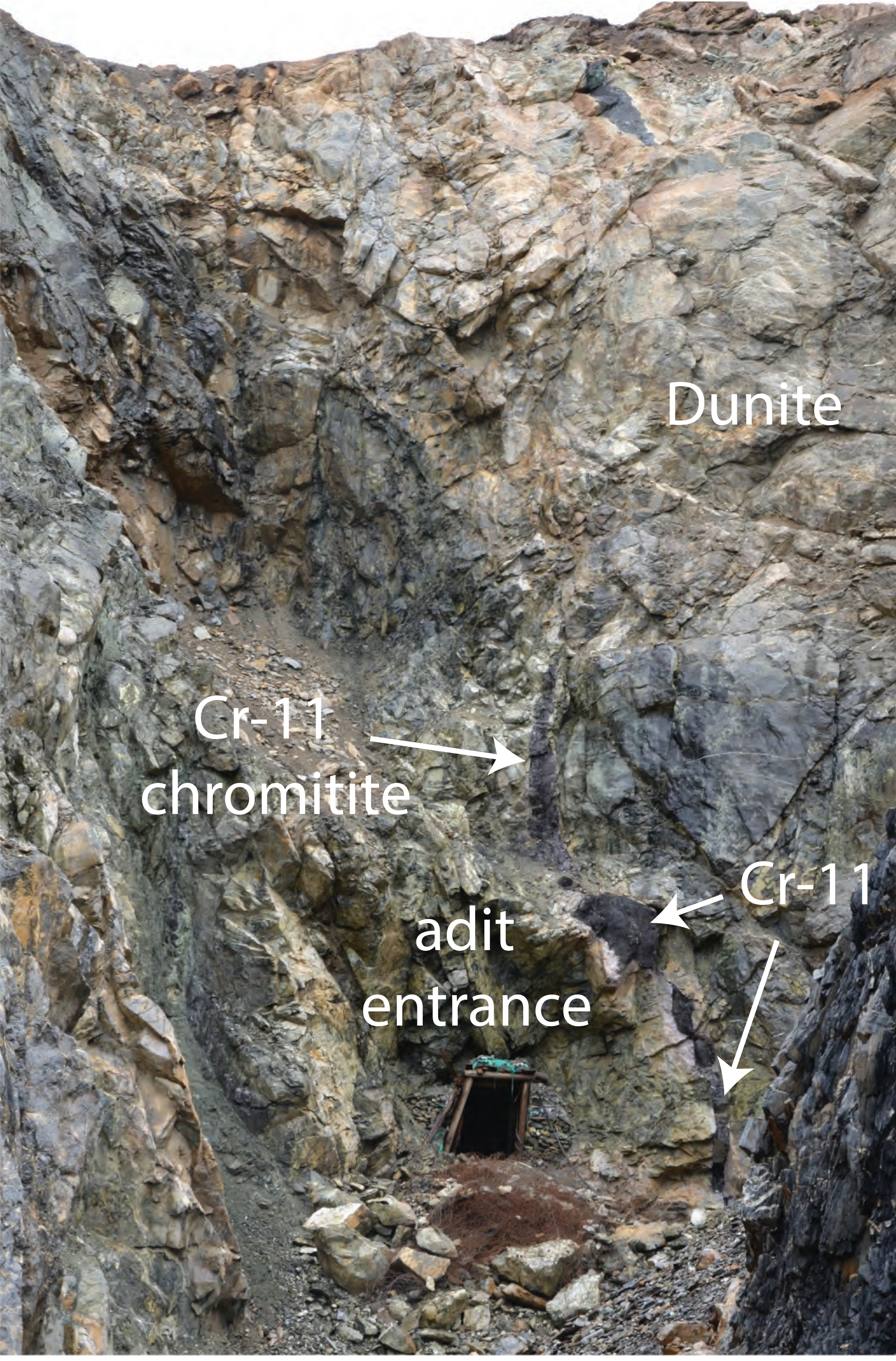

Figure 2 ms 7647

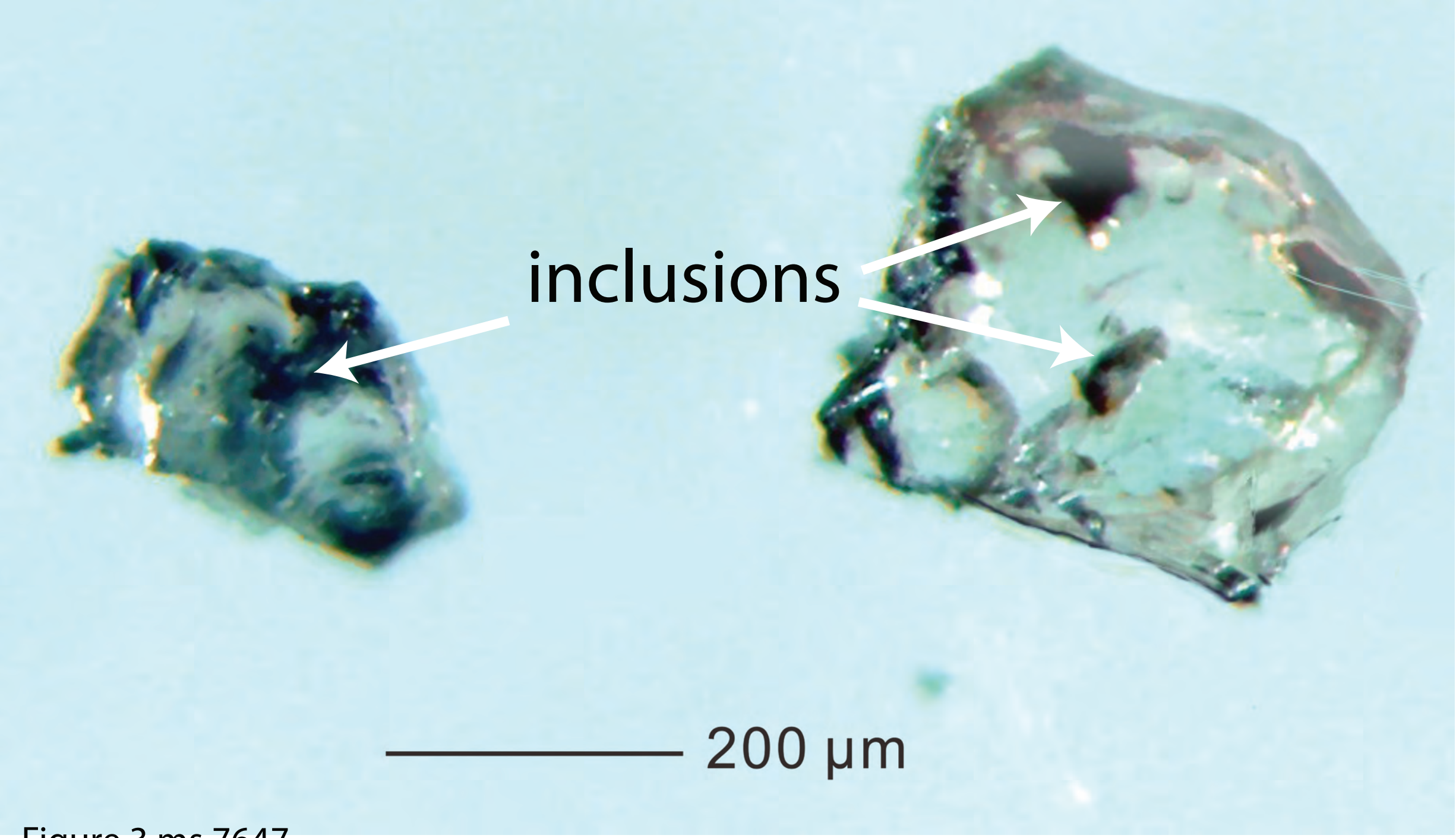

Figure 3 ms 7647

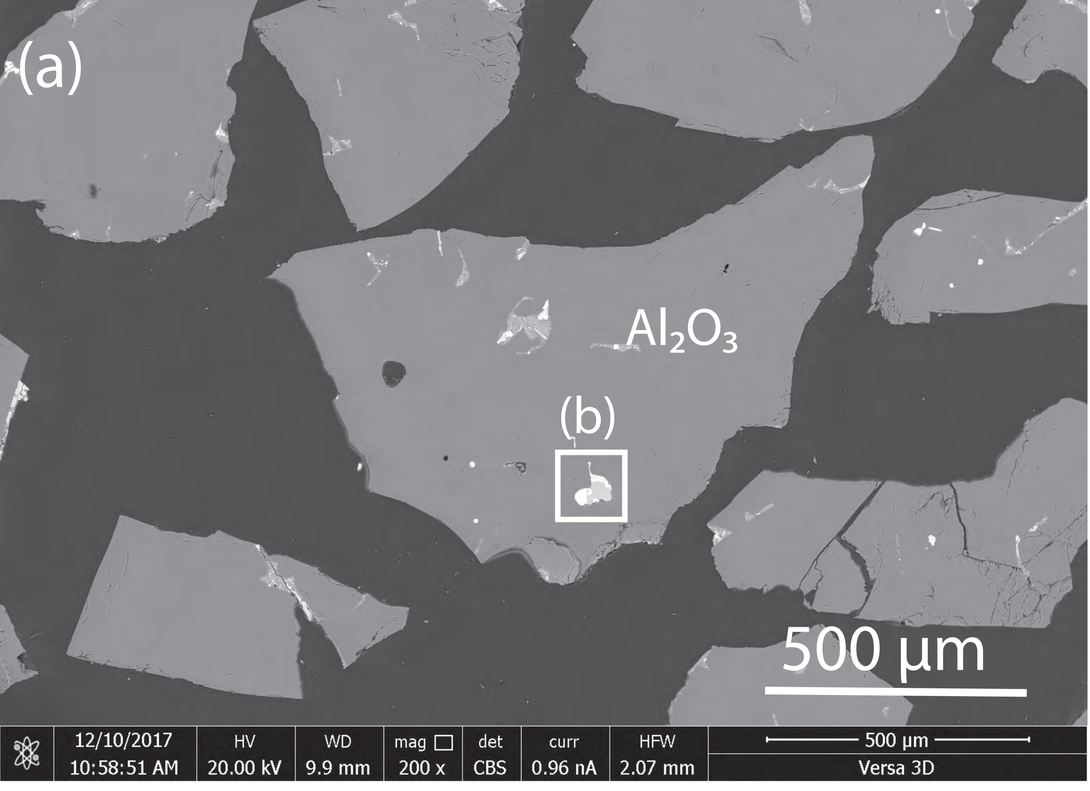

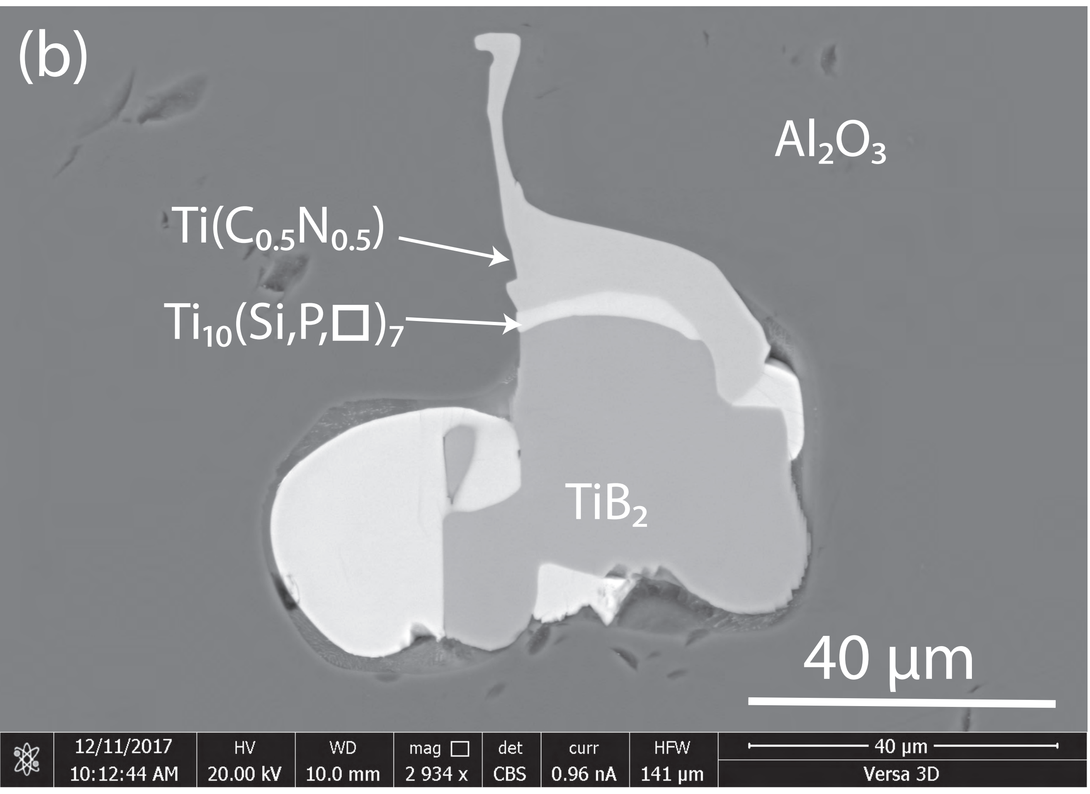

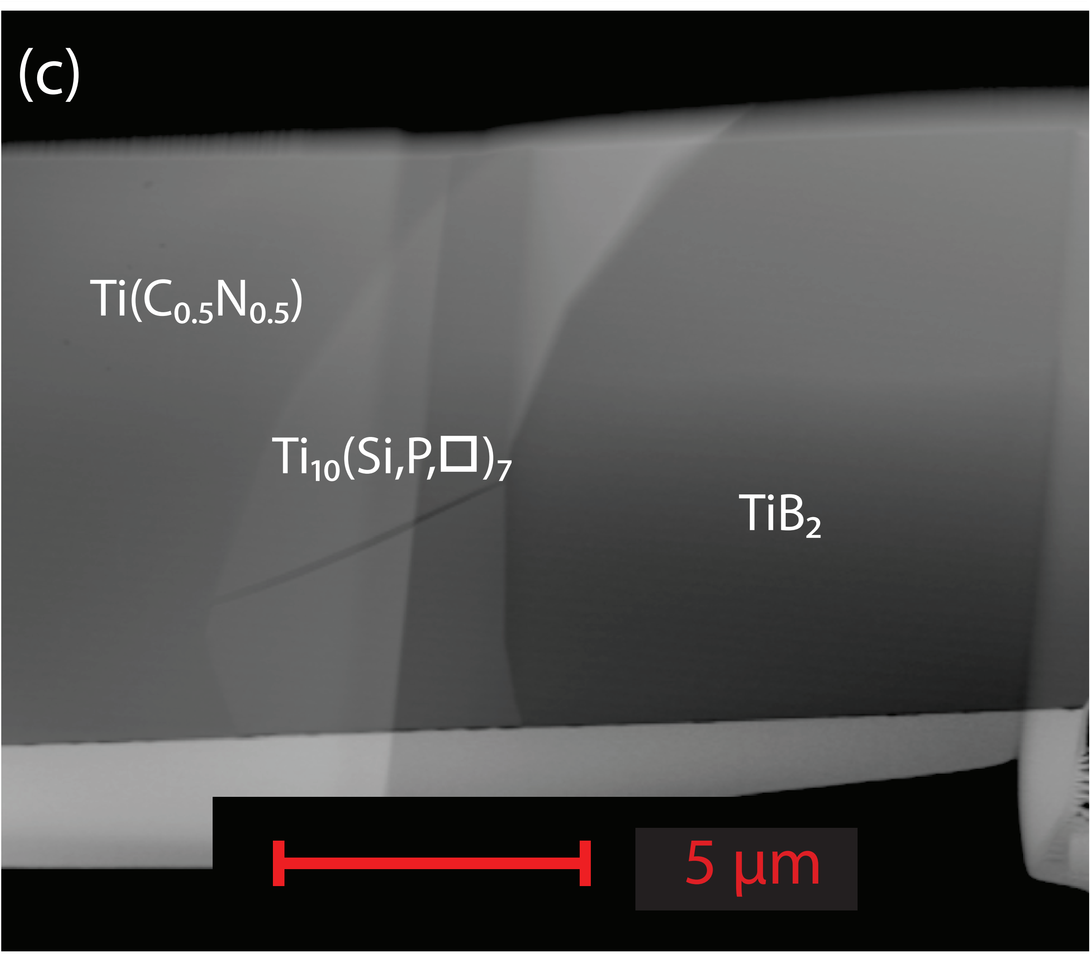

Figure 4 ms 7647

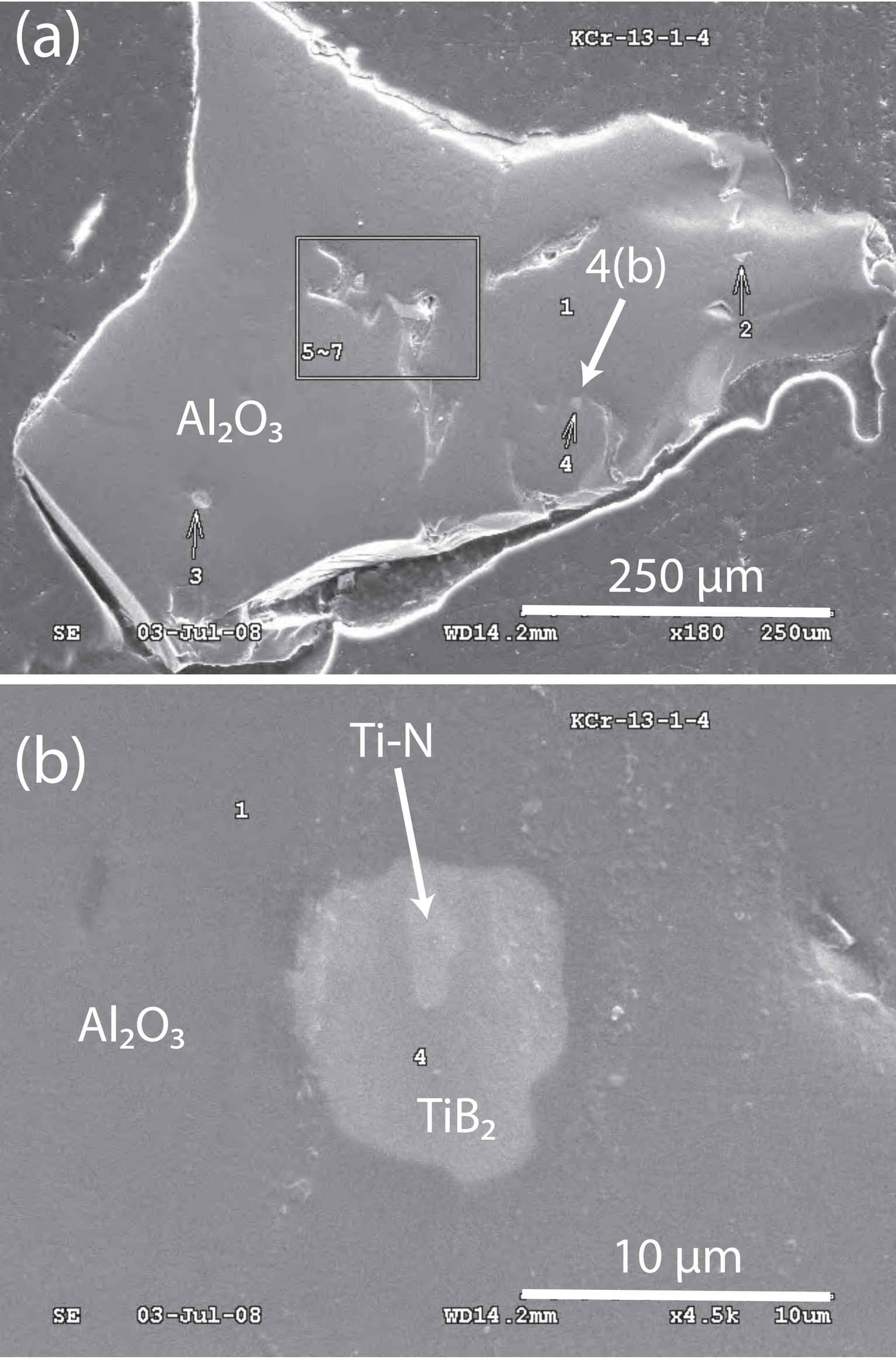

Figure 5 ms 7647

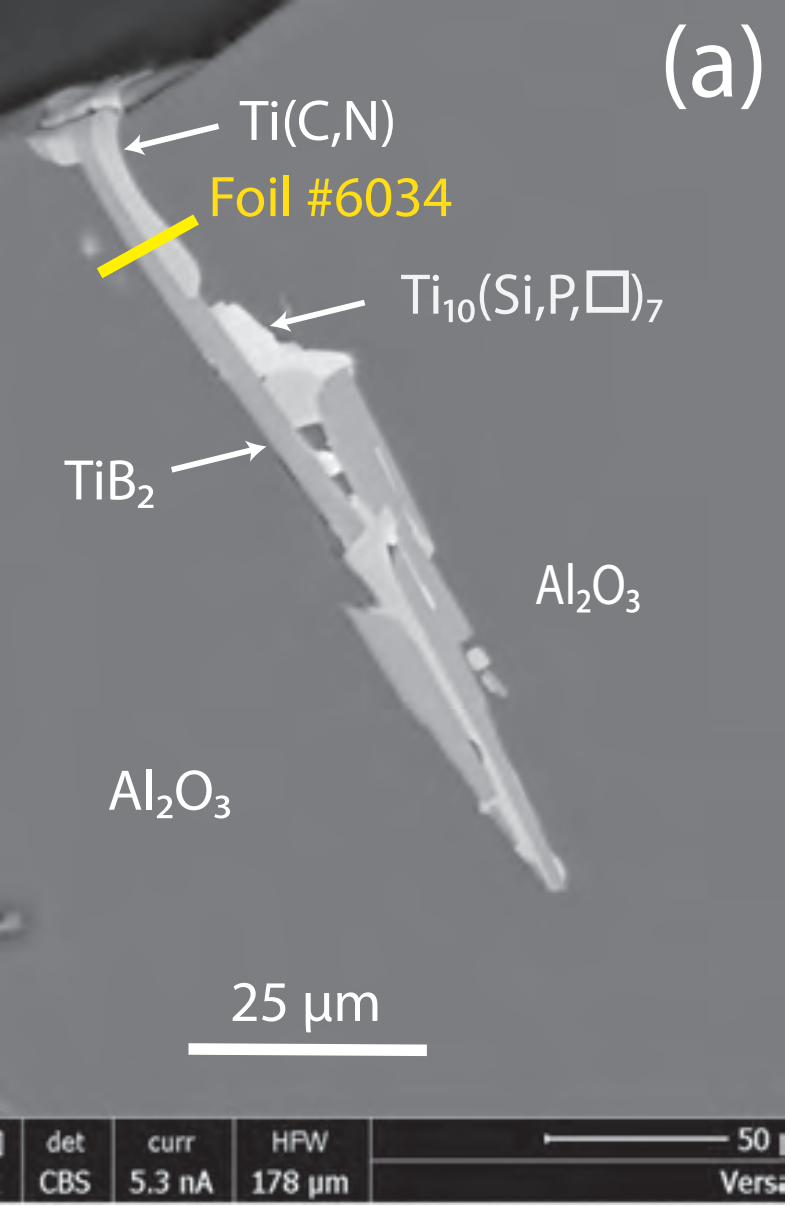

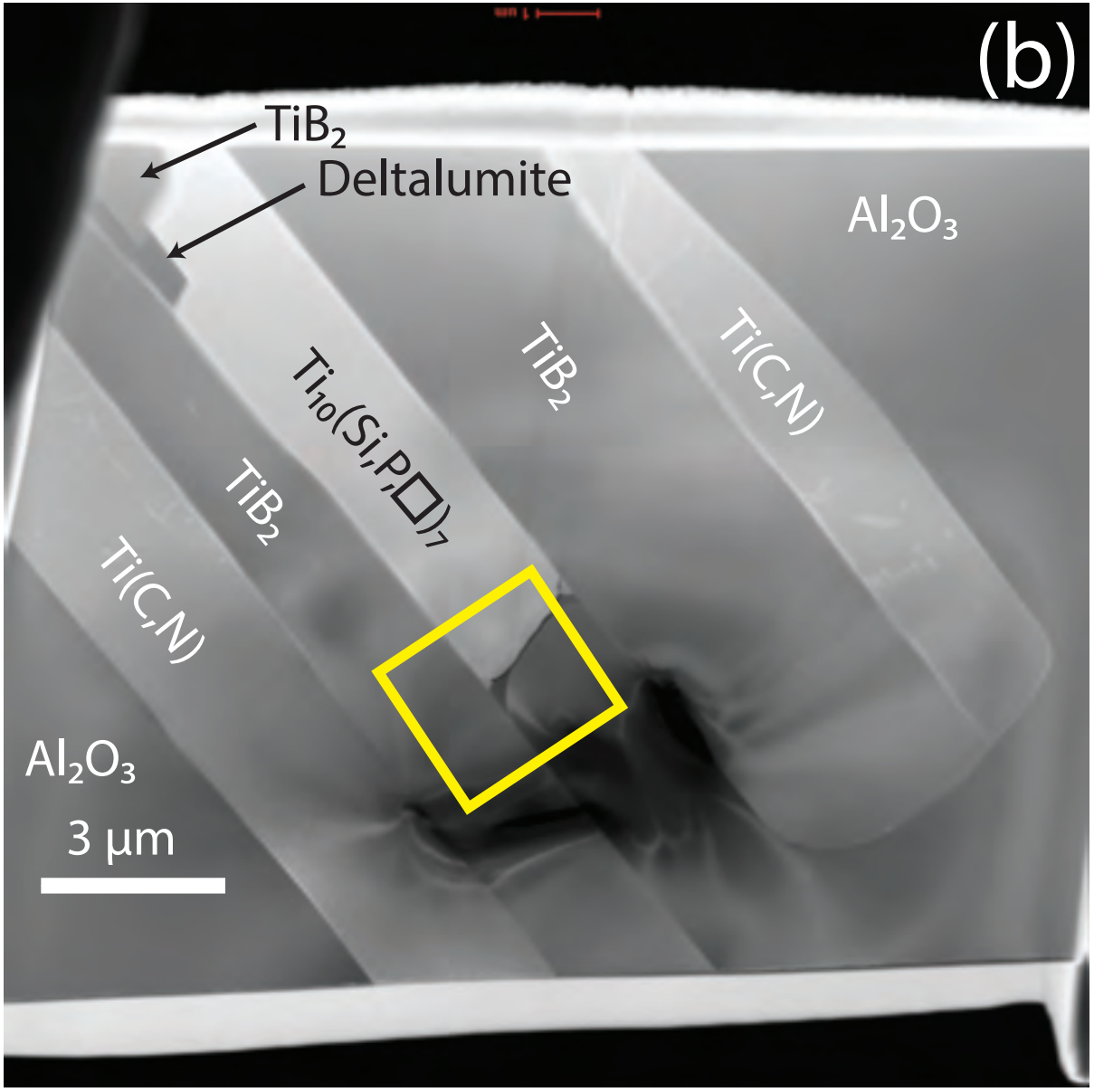

Figure 6 ms 7647

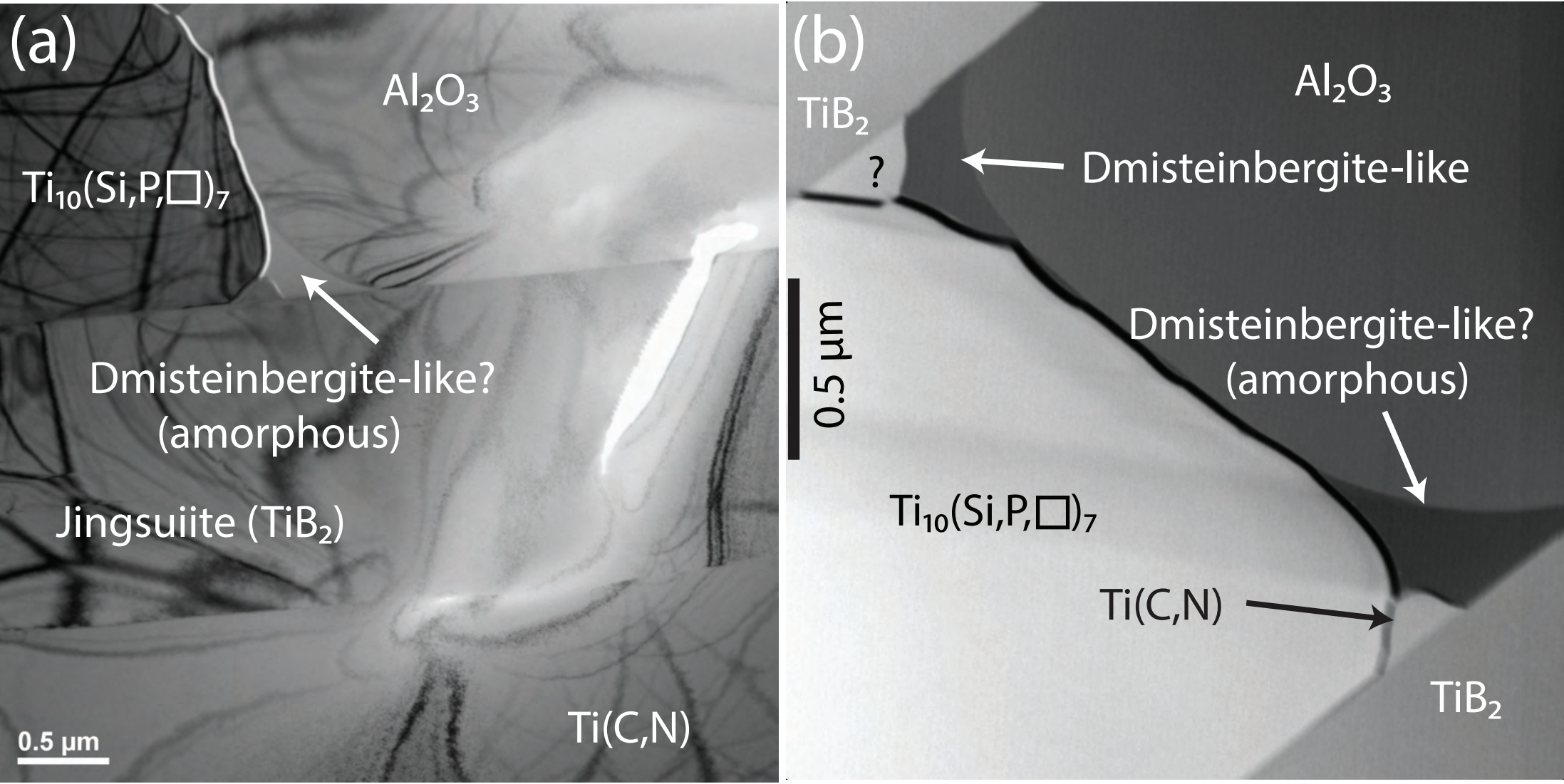

Figure 7 ms 7647

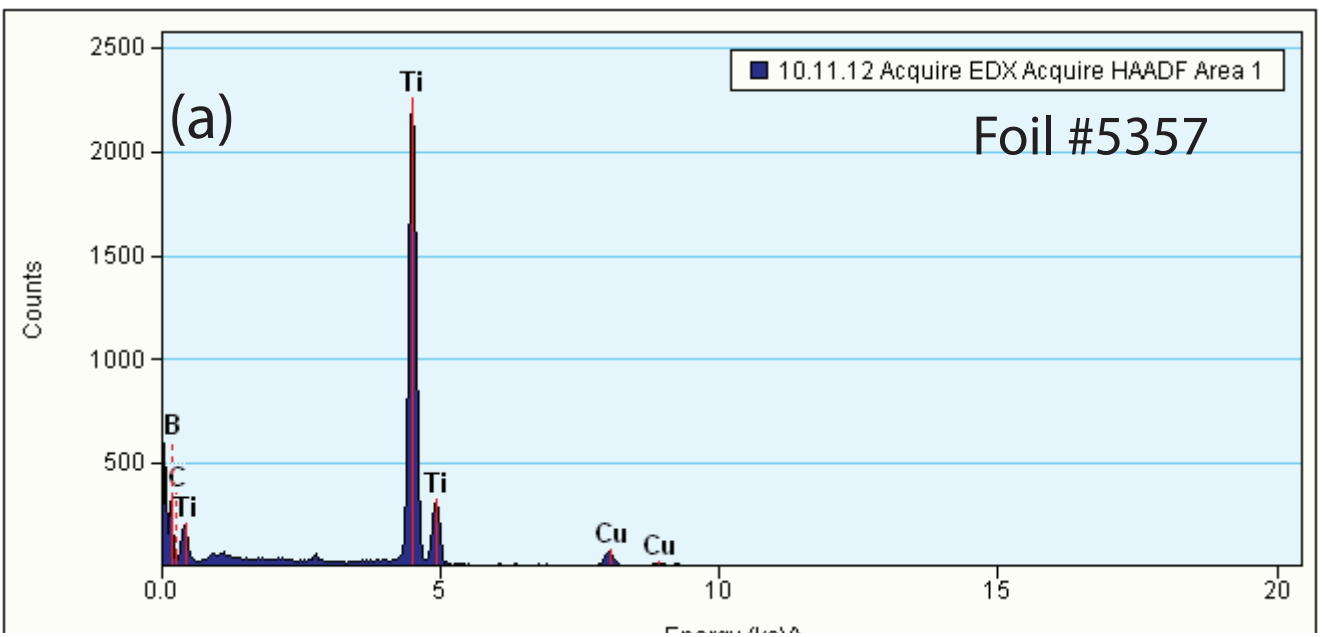

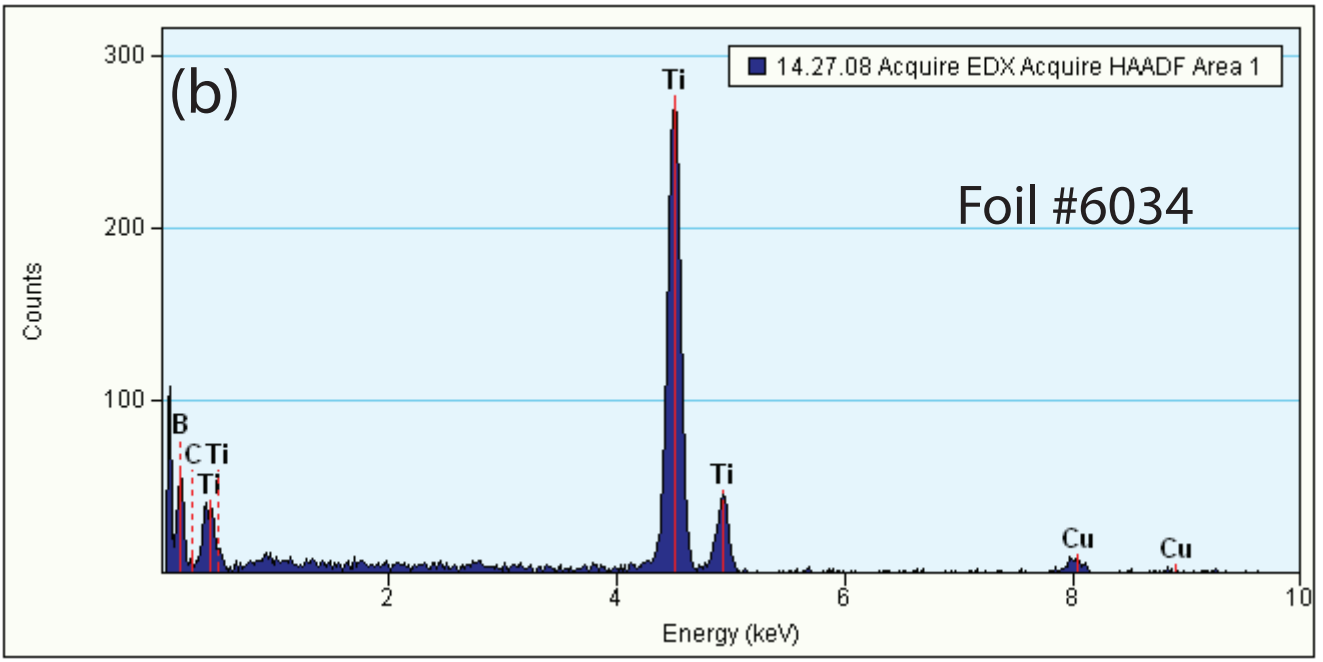

Figure 8 ms 7647

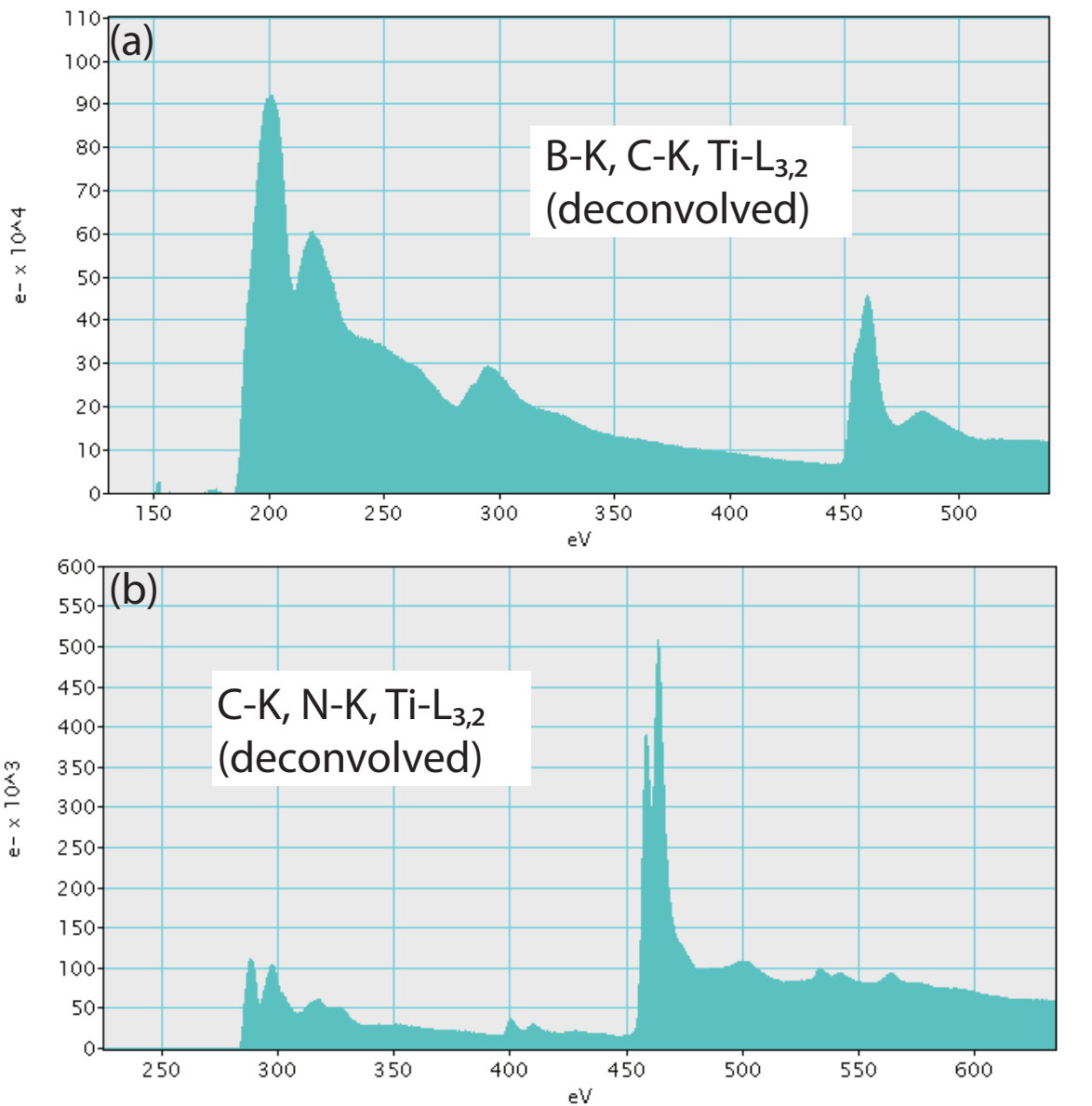

Figure 9 ms 7647

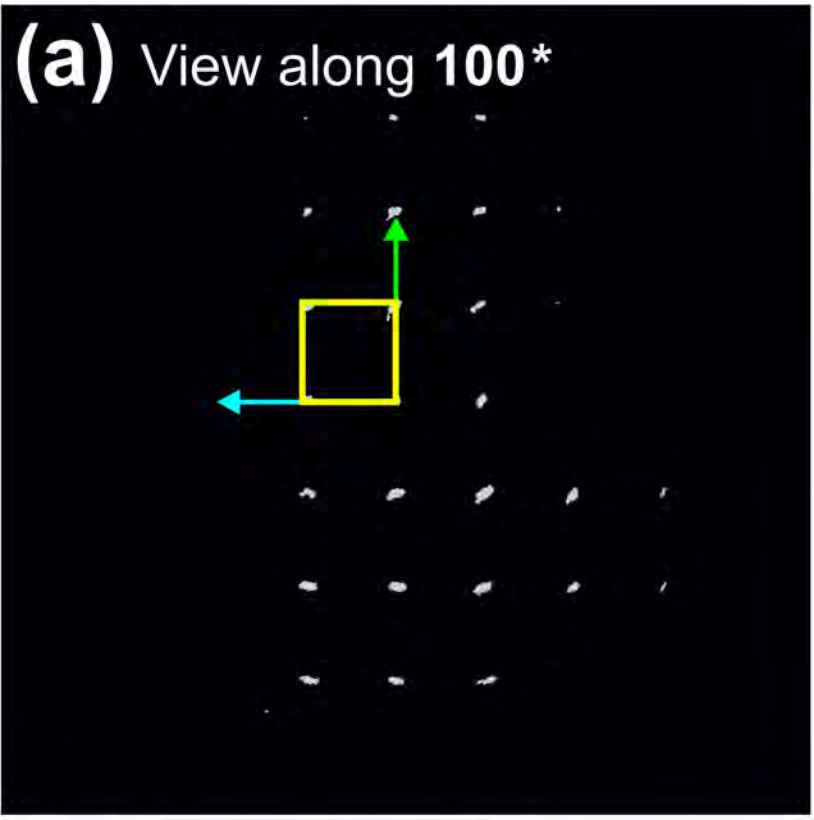
(a) View along 100*

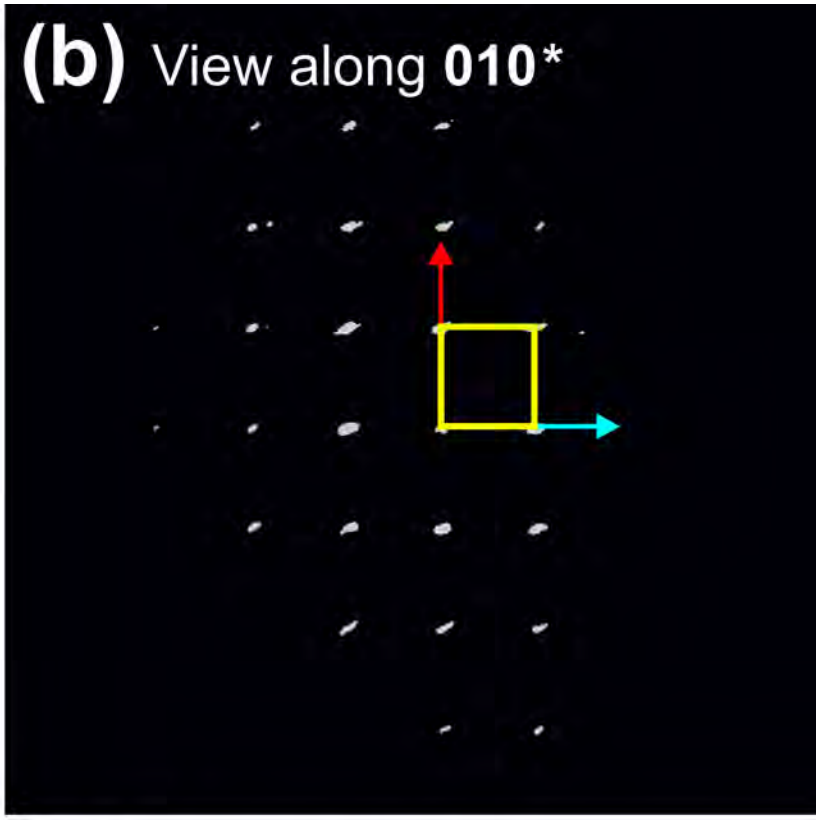
(b) View along 010*

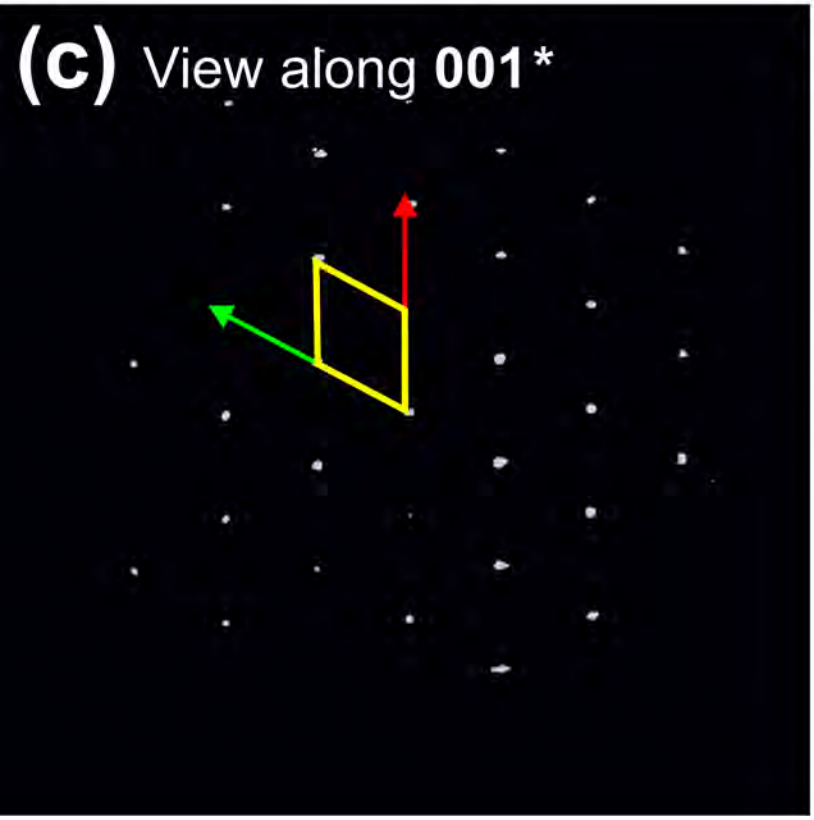
(c) View along 001*

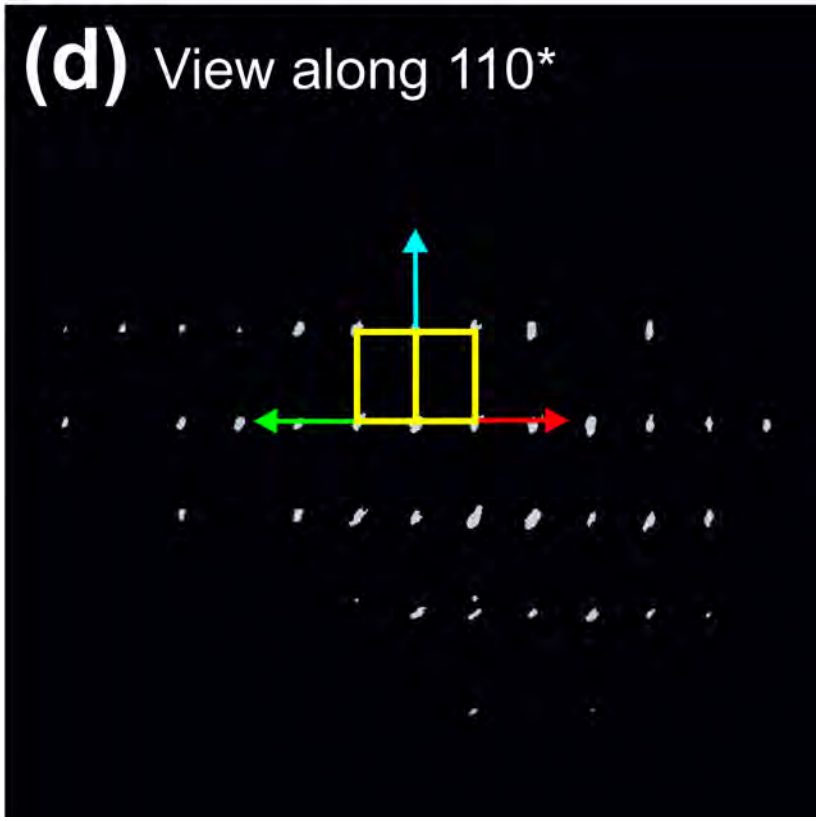
(d) View along 110*

(a)

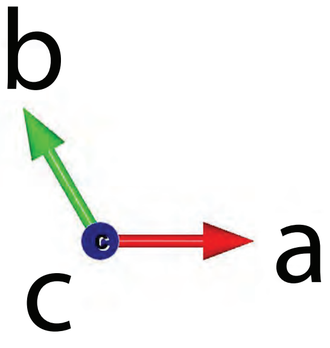

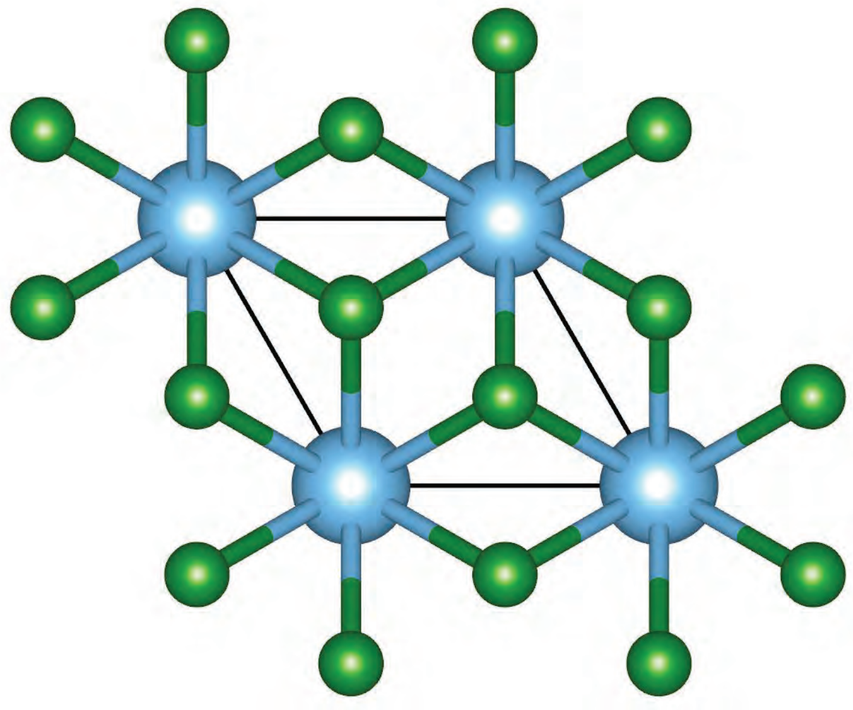

(b)

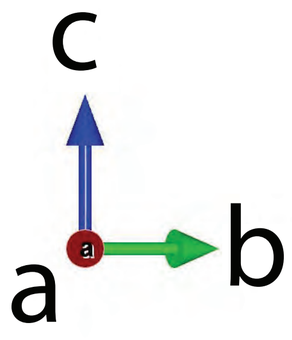

H
A
H
A
H

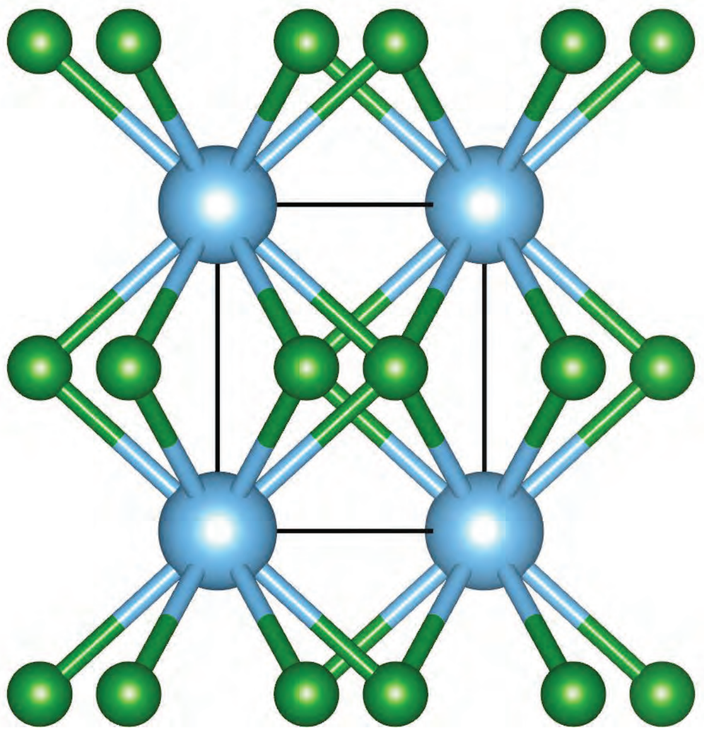

Figure 11 ms 7646

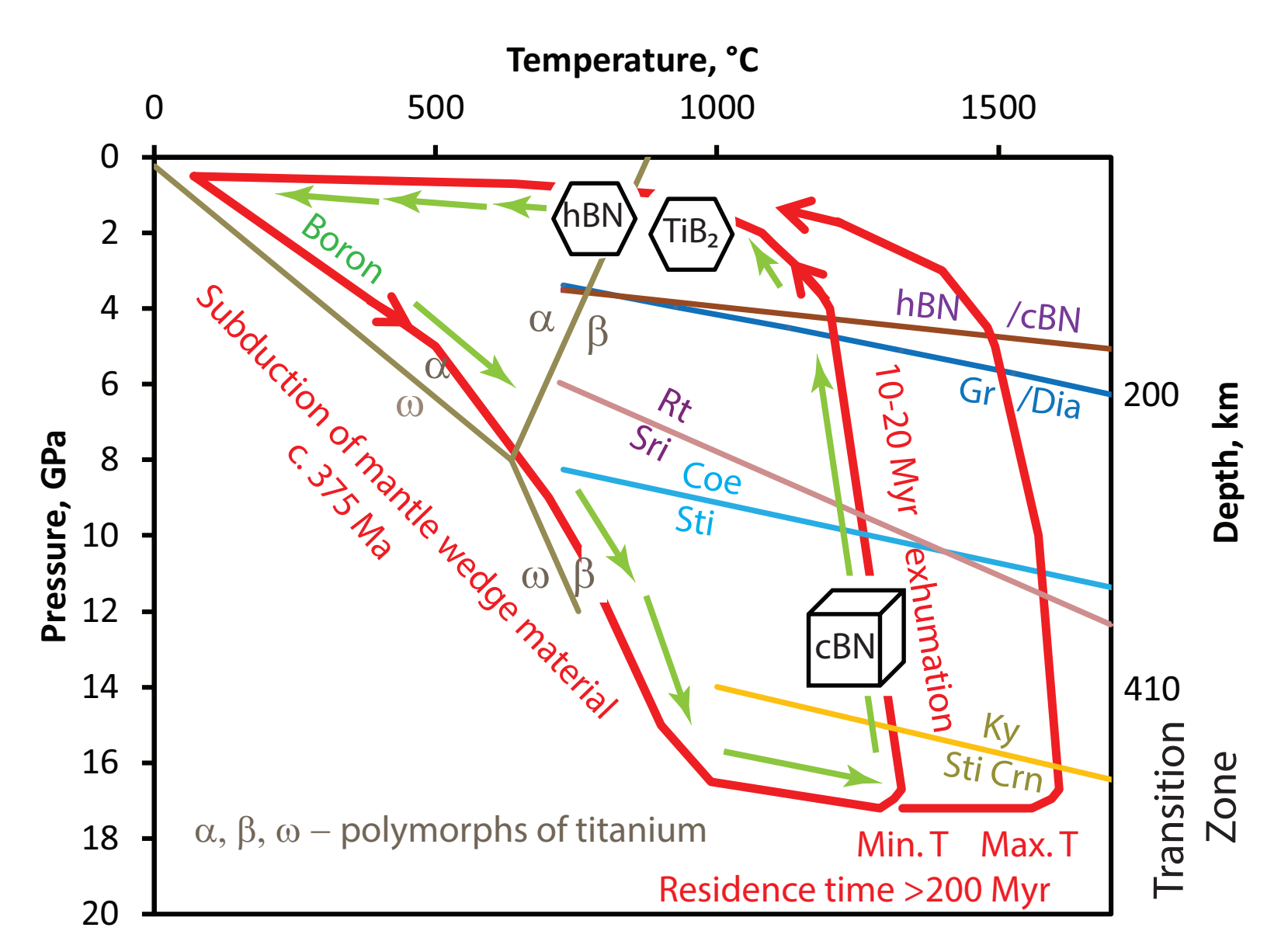

Figure 12 ms 7647